THEORETICAL ANALYSIS OF ULTRASONIC LINEAR PHASED ARRAYS FOR HYPERTHERMIC TREATMENT

BY

KENNETH BLAIR OCHELTREE

B.S., Virginia Polytechnic Institute and State University, 1982

THESIS

Submitted in partial fulfillment of the requirements
for the degree of Master of Science in Electrical Engineering
in the Graduate College of the
University of Illinois at Urbana-Champaign, 1984

Urbana, Illinois

ACKNOWLEDGEMENTS

The author would like to thank Professor Leon Frizzell and Professor Charles Cain for their work that made this thesis possible. Thanks are given to Mr. Paul Benkeser for his background work and continued assistance. Mr. Micheal Haney and Dr. Steven Foster are to be thanked for their many helpful suggestions and their assistance in solving software problems. Grateful acknowledgement is given to those who helped with the preparation of this thesis. Finally, the author would like to thank his parents for their support and encouragement.

TABLE OF CONTENTS

CHAPTER 1

INTRODUCTION

Hyperthermia has recently gained recognition as a clinical tool for treating tumor tissue, usually as an adjunct to chemotherapy or radiation treatment. Any of several types of applicators may be used to provide the necessary heating, including radio frequency, microwave and ultrasound [Lele, 1980; Hynynen et al., 1981]. Of these microwaves and ultrasound are increasingly used, each presenting advantages in different situations. Ultrasound is excellent for heating, including heating of deep structures, in areas unobstructed by gas or bone. At frequencies which provide the appropriate heat generation rates in tissue, ultrasonic waves have a smaller wavelength than microwaves and consequently can be focused more easily for localized hyperthermic treatment [Christensen and Durney, 1981]. For this reason ultrasound is being used increasingly for local hyperthermia.

Ultrasound has traditionally been applied by fixed focus applicator systems which have to be adjusted by hand prior to treatment and mechanically moved to change the location of the focus [Lele, 1980]. The use of a phased array for applying the ultrasound offers the advantage of relying on electronic rather than mechanical means to move the ultrasound beam and allows for arbitrary scanning patterns that can be made to conform to the shape and size of the tumor.

An ultrasonic phased array for hyperthermia would generally be operated in a continuous wave (cw) mode to provide the power

necessary for large heating rates. The phase of the signal applied to each element of the array could be controlled digitally by the use of counters [Benkeser, 1983]. The array surface should be as large as practical to provide sufficient power generation with adequate heat dissipation for the source. However, there are other design parameters that are not as easily specified. These include deciding between a one dimensional and a two dimensional array, choosing element dimensions and separation and determining the number of bits necessary for adequate phase resolution in the digital phase control system.

This thesis deals with the theoretical computation of the field quantities and heat generation rates produced by a phased array applicator. The model developed allows theoretical determination of the parameters which produce the ultrasonic field such that it meets the design criteria. Briefly, some of the design specifications include the limits of the treatment area, the focal size, and the magnitude of any off focus maxima in the field. Specifically, the treatment area and therefore the area scanned by the array should be a minimum of 100 mm by 100 mm. The 3 dB beam width at the focus should not exceed 20 mm. The intensity and thus heating rate at the focus should be at least 3 dB greater than at any other point in the field for all beam locations.

The remainder of this thesis is organized as follows. In Chapter 2 several methods are described that can be used to calculate the field produced by an ultrasonic array. In Chapter 3 the calculation of heating rate from a knowledge of the pressure field or element source power is detailed. In Chapter 4 the

accuracy necessary for the digital phasing system is determined. The possibility of using phase shifts to reduce grating lobes is explored in Chapter 5. Recommendations for future work are presented in Chapter 6.

CHAPTER 2

MODELLING THE FIELD PRODUCED BY THE ARRAY

2.1 Theory

The design of an ultrasonic phased array requires a means of examining and comparing various array configurations. The ultimate test of a hyperthermia phased array design is to construct the array and measure its field and heat production. However, many different array designs need to be investigated and many parameters determined. Fabricating all possible array designs would be too time consuming and expensive so a theoretical method of evaluating different array designs is necessary. The approach is to determine, from the calculated acoustic field, the proper choice of parameters to meet the design specifications given in Chapter 1.

Several different methods of calculating the pressure distribution due to a phased array are examined in this chapter in order to determine the most efficient method. The pressure distribution was calculated rather than the more meaningful quantity of heat generation rate since there is a simple relationship between them.

The problem of finding the pressure field for a plane phased array is a special case of the problem of finding the radiation field produced by an arbitrary source set in an infinite baffle [Kinsler et al., 1982]. For such a source, each infinitesimal element of area dS on the source contributes dp of pressure given by

$$dp = \frac{j\rho ck}{2\pi r} (u \cdot dS) e^{j(\omega t - kr)} \qquad (2.1)$$

where ρ is the density of the medium, c is the sound speed in the medium, k is the wave number (2π divided by the wavelength), r is the distance from dS to the point in the field where dp is being calculated, and u is the complex velocity distribution of the surface S. If the propagation medium has an attenuation coefficient α, Eq. (2.1) must be modified to give

$$dp = \frac{j\rho ck}{2\pi r} (u \cdot dS)\ e^{-\alpha r}\ e^{j(\omega t - kr)} \quad . \qquad (2.2)$$

For the geometry shown in Fig. 2.1 with S lying in the x - y plane (z = 0 plane), the total pressure is

$$p = \frac{j\rho cke^{j\omega t}}{2\pi} \int_S u(x_o, y_o)\ \frac{e^{-(\alpha + jk)r}}{r}\ dS \qquad (2.3)$$

where $u(x_o, y_o) = u_o(x_o, y_o) \exp(j\beta(x_o, y_o))$ and $u_o(x_o, y_o)$ and $\beta(x_o, y_o)$ are the magnitude and phase angle, respectively, of the surface velocity of the element at (x_o, y_o). Since the actual pressure is the real part of Eq. (2.3), the time dependence can be dropped and the magnitude of the remaining expression will give the pressure amplitude. Actual pressure is obtained by multiplying the pressure amplitude by $\cos(\omega t + \gamma)$ where γ is the phase angle from Eq. (2.3) with time dependence removed. The pressure amplitude provides all the necessary field information

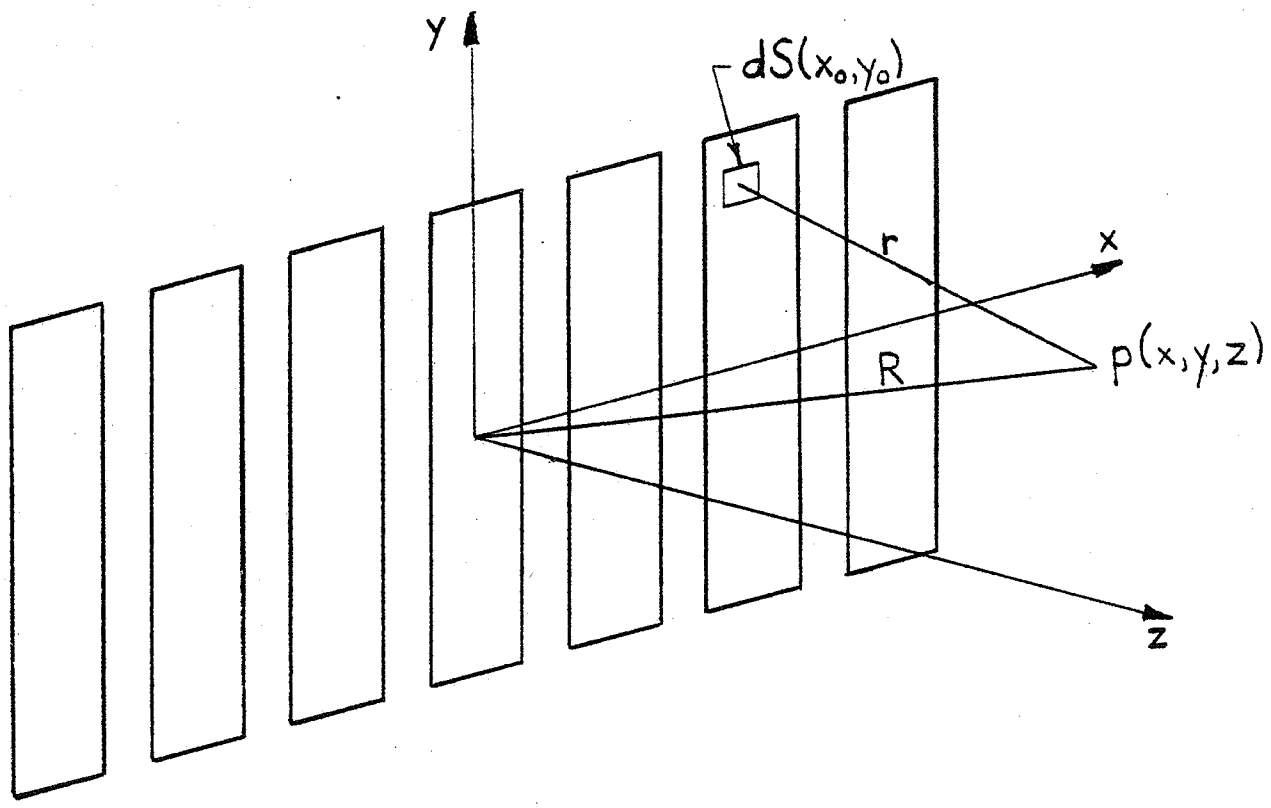

Figure 2.1 Array Geometry

and is given by the magnitude of the expression

$$p_o = \frac{j\rho ck}{2\pi} \int_S u(x_o,y_o)\frac{e^{-(\alpha+jk)r}}{r}\, dS \quad . \tag{2.4}$$

Equation (2.4) can be evaluated using several different numerical approximations which are discussed in the remainder of this chapter.

2.1.1 Fourier Transform Method

The efficiency of the Fast Fourier Transform (FFT) algorithm has led to its utilization in the calculation of acoustic fields [Stepanishen and Benjamin, 1981; Williams and Maynard, 1982]. Care must be taken to ensure that the transform is used correctly, i.e., the source is sampled sufficiently and zero padding is done correctly. An application of the transform for field calculations follows.

For the geometry illustrated in Fig. 2.1, the appropriate value for r may be substituted into Eq. (2.4) and $u(x_o,y_o)$ defined on the entire x - y plane such that it is equal to zero for points not on the array yielding the expression

$$p_o = \frac{j\rho ck}{2\pi} \int_{-\infty}^{\infty}\int_{-\infty}^{\infty} u(x_o,y_o)\, \frac{e^{-(\alpha+jk)\sqrt{(x-x_o)^2 + (y-y_o)^2 + z^2}}}{\sqrt{(x-x_o)^2 + (y-y_o)^2 + z^2}}\, dx_o dy_o \tag{2.5}$$

which can be immediately recognized as a convolution integral. Using the operator ** to represent a two dimensional convolution over x and y, Eq. (2.5) can be rewritten as

$$p_o = \frac{j\rho ck}{2\pi} \left[u(x,y) \;**\; \frac{e^{-(\alpha+jk)\sqrt{x^2+y^2+z^2}}}{\sqrt{x^2+y^2+z^2}} \right] \quad . \tag{2.6}$$

Since the Fourier transform of the convolution of two functions is the product of the functions, the use of the Fourier transform simplifies the evaluation of the equation. Let F_x, F_y, and F_{xy} be the Fourier transforms over x, over y, and over x and y, respectively. For a linear array, u(x,y) is separable in x and y, i.e., u(x,y) is the product of $u_x(x)$ and $u_y(y)$. Then, $P_o(\omega_1,\omega_2)$, $U(\omega_1,\omega_2)$, $U_x(\omega_1)$, and $U_y(\omega_2)$ can be represented by $F_{xy}\{p_o\}$, $F_{xy}\{u\}$, $F_x\{u_x\}$, and $F_y\{u_y\}$, respectively. Transforming Eq. (2.6) and using the separability of u(x,y) gives

$$P_o(\omega_1,\omega_2) = \frac{j\rho ck}{2\pi} U_x(\omega_1)U_y(\omega_2) \quad F_{xy}\left\{ \frac{e^{-(\alpha+jk)\sqrt{x^2+y^2+z^2}}}{\sqrt{x^2+y^2+z^2}} \right\} \quad . \tag{2.7}$$

The pressure p_o is simply the inverse Fourier transform of Eq. (2.7) or

$$p_o(x,y) = \frac{j\rho ck}{2\pi} \quad F_{xy}^{-1}\left[U_x(\omega_1)U_y(\omega_2) \quad F_{xy}\left\{ \frac{e^{-(\alpha+jk)\sqrt{x^2+y^2+x^2}}}{\sqrt{x^2+y^2+z^2}} \right\} \right] \tag{2.8}$$

A circular convolution can be evaluated numerically using a Fast Fourier Transform (FFT) algorithm, but Eq. (2.6) contains a linear convolution. The array geometry is specified for the FFT by providing the complex velocity values for a matrix of points on

the surface of the array. For a linear convolution to be evaluated using a circular convolution, the data matrix must be padded with zeros so there is no wraparound effect [Oppenheim and Schafer, 1975]. Padding must be done with a number of zeros equal to the number of data points in each direction of the data matrix. For a two dimensional matrix of data points, the padded matrix will contain twice the number of points in both the x and y directions as the original data matrix and, therefore, will include four times the number of points found in the original data matrix. Evaluating Eq. (2.8) using the FFT will not give just one pressure point, but will give values for an array of points in a constant z plane located at the same x and y positions as the points at which the array was specified and extending into the zero padded area surrounding the array.

An example of the number of points necessary when using this method can be illustrated by the examination of an array operated at 600 kHz, having a corresponding wavelength of $\lambda = 2.5$ mm, with maximum dimensions of 50 mm by 50 mm. For a sampling increment of one sixth of a wavelength, sufficient to satisfy the Nyquist sampling criterion, the array would be represented by 120 by 120 nonzero points in the x - y plane. Padding the data with an equal number of zeros gives a field of 240 by 240 points, but since an FFT requires a number of points that is an integer power of 2, an array of 256 by 256 points must be used.

To evaluate the pressure using this method, $U_x(\omega_1)$ and $U_y(\omega_2)$ first need to be evaluated by transforming $u_x(x)$ and $u_y(y)$ using one dimensional FFTs with sufficient zero padding. $U_x(\omega_1)$ could be calculated numerically by assuming $u_x(x)$ is a rectangle

function of length h and since $U_x(\omega_1)$ is the Fourier transform of a rectangle function

$$U_x(\omega_1) = \frac{2\sin\left(\frac{\omega_1 h}{2}\right)}{\omega_1} \quad . \tag{2.9}$$

For an array of equal element spacings s, element widths w, complex surface velocities u_n, and number of elements N, centered on the y axis

$$u_y(y) = \sum_{n=1}^{N} u_n \text{rect}\left(y + \frac{s(N+1)}{2} - ns\right) \tag{2.10}$$

$$U_y(\omega_2) = \sum_{n=1}^{N} \frac{2\sin\left(\frac{\omega_2 w}{2}\right)}{\omega_2} u_n e^{-j\omega\left(\frac{s(N-1)}{2} - ns\right)} \quad . \tag{2.11}$$

Thus, $U_x(\omega_1)$ and $U_y(\omega_2)$ can be calculated numerically by using an FFT or analytically by using the exact transform expressions.

A two dimensional FFT needs to be used to evaluate the transform of $\exp(-(\alpha + jk)r)/r$. This transform is then multiplied by $U_x(\omega_1)U_y(\omega_2)$, the inverse two dimensional FFT is taken, and the result is multiplied by the constant $j\rho ck/2\pi$ to give the pressure p_o.

A lower limit on the time required for such a program to run can be obtained by assuming that the FFT calculations require the majority of computer time. Assuming that the multiplication operations in the FFT calculation are the most time consuming allows the run time to be calculated since for an FFT of length N

there are $N\log_2 N$ multiplications. If the program is implemented on the Perkin Elmer 7-32 used at the Bioacoustics Research Laboratory where a complex multiplication takes an average time of 208 microseconds, the total run time for the given example would be greater than six minutes.

Six minutes is a reasonable amount of time to calculate a constant z plane of values, but if it is desired to calculate only a set of points along the z axis, six minutes is a prohibitively long time for calculating each point. Also, as was noted, the field points calculated are at the same x and y locations as the points used to represent the hyperthermia array. In order to calculate the field points over a larger area with the same resolution, the FFT size would need to be increased; the spacing of the input points needs to be kept the same to preserve the same accuracy. Also, if it is not desired to calculate field points at the same spacing as is necessary to represent the array, then there is much wasted computation in determining the additional field points. Therefore, determining the field by exact transform is not an efficient general method.

The Fourier transform method can be applied using different approximations. The first set of approximations is known as the Fresnel approximation and assume that $z \gg x$ and $z \gg y$ so that the terms in Eq. (2.8) can be simplified as follows.

$$e^{-(\alpha+jk)\sqrt{x^2+y^2+z^2}} \simeq e^{-(\alpha+jk)\left(z + \frac{x^2}{2z} + \frac{y^2}{2z}\right)} \qquad (2.12)$$

$$\frac{1}{\sqrt{x^2 + y^2 + z^2}} \simeq \frac{1}{z} \quad . \tag{2.13}$$

Two terms of the binomial expansion for the radical are necessary in the phase term approximation (Eq. (2.12)) because an error of half a wavelength in the phase term causes the effects of the radiation from a given point to be subtractive rather than additive. Applying the approximations yields

$$F_{xy}\left\{\frac{e^{-(\alpha+jk)\sqrt{x^2+y^2+z^2}}}{\sqrt{x^2+y^2+z^2}}\right\} = \frac{e^{-(\alpha+jk)z}}{z} F_x\left\{e^{-(\alpha+jk)\frac{x^2}{2z}}\right\} F_y\left\{e^{-(\alpha+jk)\frac{y^2}{2z}}\right\} . \tag{2.14}$$

This rearrangement is possible because the function becomes separable in x and y when the approximations are applied. Using the transform $F_x\{\exp(-x^2/2\sigma^2)\} = \sigma(2\pi)^{\cdot 5}\exp(-\sigma^2\omega_1{}^2/2)$ gives

$$F_{xy}\left\{\frac{e^{-(\alpha+jk)\sqrt{x^2+y^2+z^2}}}{\sqrt{x^2+y^2+z^2}}\right\} = \frac{2\pi}{\alpha+jk} e^{-(\alpha+jk)z - \frac{z(\omega_1^2+\omega_2^2)}{2(\alpha+jk)}} \tag{2.15}$$

Substituting this expression into Eq. (2.8) yields

$$p_o(x,y) = \frac{j\rho kc}{\alpha+jk} F_{xy}^{-1}\left\{U_x(\omega_1)U_y(\omega_2)\, e^{-(\alpha+jk)z - \frac{z(\omega_1^2+\omega_2^2)}{2(\alpha+jk)}}\right\} . \tag{2.16}$$

Thus, using the Fresnel approximations, a form for the pressure is obtained containing only one two dimensional FFT. The accuracy of

this approximation will be discussed after the Fraunhofer approximation is examined.

The Fraunhofer approximation uses the distance from the origin R in its approximations by assuming that $R >> x_o$ and $R >> y_o$. Thus,

$$e^{-(\alpha+jk)\sqrt{z^2+(x-x_o)^2+(y-y_o)^2}} = e^{-(\alpha+jk)\sqrt{R^2-2xx_o-2yy_o+x_o^2+y_o^2}} \quad . \tag{2.17}$$

Using the first two terms of a binomial expansion of the radical yields

$$e^{-(\alpha+jk)\sqrt{z^2+(x-x_o^2)+(y-y_o^2)}} \simeq e^{-(\alpha+jk)\left(R-\frac{xx_o}{R}-\frac{yy_o}{R}+\frac{x_o^2}{2R}+\frac{y_o^2}{2R}\right)} \quad . \tag{2.18}$$

For $kx_o^2/2R + ky_o^2/2R$ small compared to π, omission of these terms produces a negligible phase error and gives the expression

$$e^{-(\alpha-jk)\sqrt{z^2+(x-x_o)^2+(y-y_o)^2}} \simeq e^{-(\alpha+jk)\left(R-\frac{xx_o}{R}-\frac{yy_o}{R}\right)} \tag{2.19}$$

Using Eq. (2.19), assuming $1/r \approx 1/R$ and substituting into Eq. (2.4) yields

$$p_o = \frac{j\rho ck}{2\pi}\int_S u_x(x_o)u_y(y_o)\,\frac{e}{R}^{-(\alpha+jk)\left(R-\frac{xx_o}{R}-\frac{yy_o}{R}\right)}\,dS \quad . \tag{2.20}$$

Taking advantage of the separability of u(x,y) leads to

$$p_o = \frac{j\rho ck}{2\pi R} e^{-(\alpha+jk)R} \int_{-\infty}^{\infty} u_x(x_o)\, e^{(\alpha+jk)\frac{xx_o}{R}}\, dx_o \int_{-\infty}^{\infty} u_y(y_o)\, e^{(\alpha+jk)\frac{yy_o}{R}}\, dy_o \quad . (2.21)$$

Assuming that the attenuation term in the integrals can be neglected and noting that the two remaining integrals represent Fourier transforms gives

$$p_o = \frac{j\rho ck}{2\pi R} e^{-(\alpha+jk)R}\, U_x\left(\frac{-kx}{R}\right) U_y\left(\frac{-ky}{R}\right) \quad . \qquad (2.22)$$

Thus, the Fraunhofer approximation requires the evaluation of the transforms of u_x and u_y (Eq. (2.9) and Eq. (2.11)). If an FFT is used to evaluate U_x and U_y, then the points at which the field is calculated will be spaced by $2\pi R/kN\Delta x$ where N is the FFT size in the x direction and Δx is the sampling increment on the array. For the sampling increment of the previous example with Δx equal to one sixth of a wavelength, the points in the fields are spaced by 6R/N. For a typical N, i.e., N = 256, the field spacing is 0.023R; for a given N the spacing of the field points is proportional to the distance from the array.

The major difference between the Fraunhofer and Fresnel approximations is that the Fraunhofer approximation drops the $(x_o^2 + y_o^2)/2z$ term from the exponent by assuming that the source is small. Also the Fresnel approximation gives the field for a constant z plane while the Fraunhofer approximation evaluates the Field on a constant R surface.

Both approximations become inaccurate as x and y approach z in magnitude. The main source of error is the approximation used in the phase term since an error of one half of a wavelength in the approximation for r will cause the contribution to the field by an element to be destructive rather than constructive or vice versa. Errors in r for the Fresnel and Fraunhofer approximations are shown in Table 2.1 for various x and y values. Both approximations become unacceptably inaccurate for field points in the treatment field with large x and y displacements.

Thus, the Fourier transform method for finding the field pattern can be rejected. For solving the exact case the calculated field points are spaced too closely requiring excess computation time and are limited to an area which is too small. The approximate solutions require less calculation time but are not valid for a sufficiently large area.

2.1.2 Method of Equidistant Areas

The pressure can also be found by considering it as the summation of the pressures produced by the individual elements. The pressure produced by each element can be calculated by dividing the element surface into incremental areas each of which contributes an incremental pressure of a constant phase at the field point [Freedman, 1959]. The mathematical implementation of this method is discussed below.

The pressure produced at a point due to one element of size h by w is

Table 2.1 Errors in Fresnel and Fraunhofer Approximations for Various Source Point and Field Point Locations with Wavelength λ = 2.5 mm

z	x	x_o	y	y_o	Path length in wavelengths r/λ	Error in Fresnel Approximation in Wavelengths $\frac{1}{2}\left[r-\left(z+\frac{(x-x_o)^2+(y-y_o)^2}{2z}\right)\right]$	Error in Fraunhofer Approximation in Wavelengths $\frac{1}{\lambda}\left[r-\left(R-\frac{xx_o+yy_o}{R}\right)\right]$
50	0	0	0	0	20.00	0	0
50	2	- 2	2	- 2	20.13	-0.001	0.079
50	5	- 5	5	- 5	20.79	-0.015	0.190
50	10	-10	10	-10	22.98	-0.222	0.654
50	20	-20	20	-20	30.20	-2.601	1.651
100	10	-10	10	-10	41.57	-0.031	0.379
100	20	-20	20	-20	45.91	-0.443	1.308
100	30	-30	30	-30	52.46	-1.940	5.694

$$p_o = \frac{j\rho ck u_n}{2\pi} \int_o^h \int_o^w \frac{e^{-(\alpha+jk)r}}{r} dx_o dy_o \qquad (2.23)$$

where r is the distance to each incremental area given by $dx_o dy_o$ and u_n is the complex surface velocity on the contributing element. The presence of r in the integrand suggests that Eq. (2.23) might be simplified if the integration were performed in polar rather than rectangular coordinates. Consider the geometry of Fig. 2.2, which shows the projection of r, s in the figure, onto the x - y plane. $\beta_1(s)$ and $\beta_2(s)$ are the extreme angles for a given s, and s_{min} and s_{max} are the minimum and maximum s values, respectively. From these definitions the expression for p_o is found to be

$$p_o = \frac{j\rho ck u_n}{2\pi} \int_{s_{min}}^{s_{max}} \int_{\beta_1(s)}^{\beta_2(s)} \frac{e^{-(\alpha+jk)r}}{r} s d\beta ds \quad . \qquad (2.24)$$

Integrating with respect to β gives

$$p_o = \frac{j\rho ck u_n}{2\pi} \int_{s_{min}}^{s_{max}} \frac{e^{-(\alpha+jk)r}}{r} (\beta_2(s)-\beta_1(s)) s ds \quad . \qquad (2.25)$$

Defining an incremental area dA for the s integration as $dA = (\beta_2(s) - \beta_1(s))sds$, Eq. (2.25) becomes

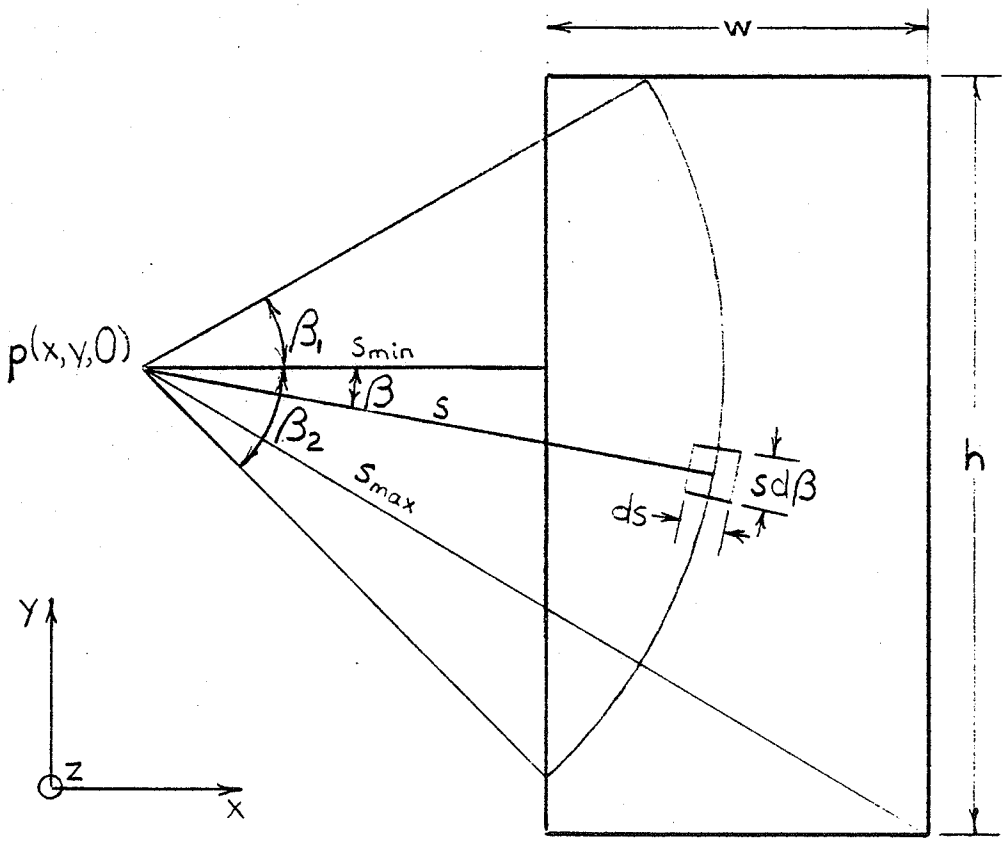

Figure 2.2 Geometry Used for Equidistant Area Method

$$p_o = \frac{j\rho ck u_n}{2\pi} \int_{s=s_{min}}^{s_{max}} \frac{e^{-(\alpha+jk)r}}{r} \, dA \quad . \tag{2.26}$$

The pressure due to the entire array can be expressed in a form that can be evaluated numerically by changing Eq. (2.26) to a summation and summing the contributions from the N array elements

$$p_o = \frac{j\rho ck}{2\pi} \sum_{n=1}^{N} u_n \sum_{s=s_{min}}^{s_{max}} \frac{e^{-(\alpha+jk)r}}{r} \Delta A \tag{2.27}$$

where $\Delta A = (\beta_2(s) - \beta_1(s))s\Delta s$ as shown in Fig. 2.3. The problem reduces to finding the area of ΔA which is the intersection of the area enclosed between two concentric circles and the area within a rectangle of size h by w.

The area between two concentric circles intersecting the area within a rectangle is found by determining the intersection of the rectangular area and the area within the larger circle and subtracting the intersection of the rectangular area and the area within the smaller circle. Thus, a simple general method is needed for the calculation of the intersection of a circular area and a rectangular area. Because there are many different ways that a circular area and a rectangular area can intersect, a method is needed that will account for all possible configurations. One procedure that works is to find the area of the circle and subtract those areas of the circle outside of the rectangle to leave the area of intersection.

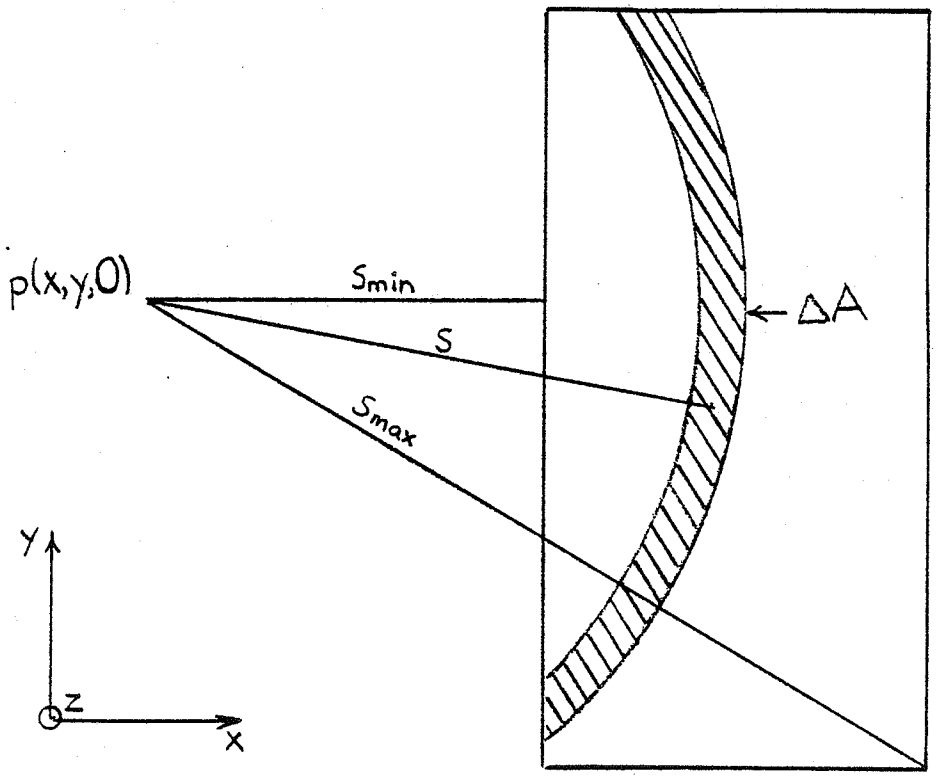

Figure 2.3 Geometry for Numerical Integration

Specifically, after the area of the circle is found, the several shaded areas shown in Fig. 2.4 are subtracted. These areas are determined from the line defining the appropriate side of the rectangle and the curve defining the circle. However, the shaded areas shown in Fig. 2.5 must be added back as they are subtracted twice by the application of the subtraction scheme as defined. The area remaining, after making these adjustments to the area of the circle, is the area of the rectangle within the circle.

The areas described in the last paragraph must be calculated from the radius of the circle, the coordinates of the circle center, the size of the element, and the location of the element. The first area to be calculated is the area of the circle which is simply πr^2.

The subtracted areas, the area defined by a chord and an arc, are found using the geometry of Fig. 2.6. The area must be expressed in terms of r and d since they are the given variables. The area of the region of interest is found by taking the area of the sector of angle Ω and subtracting the area of triangle AOB as shown in Eq. (2.28).

$$A = \frac{r^2\Omega}{2} - da \quad . \tag{2.28}$$

The variables a and Ω in terms of r and d, the given variables, are

$$a = \sqrt{r^2 - d^2} \tag{2.29}$$

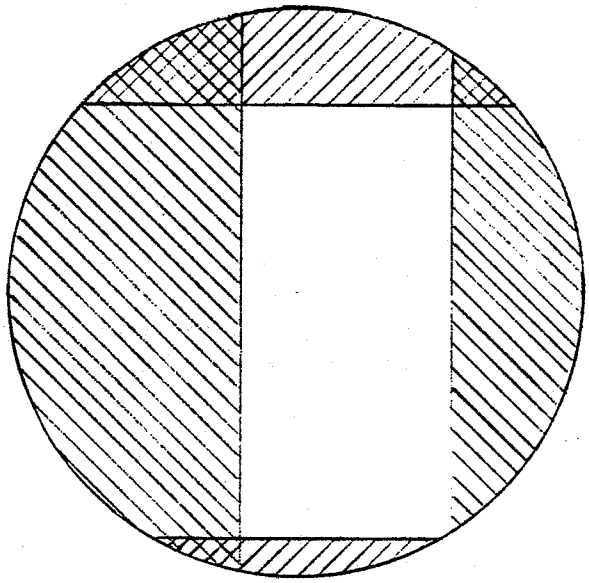

Figure 2.4 Shaded Areas Are Subtracted from Circle Area

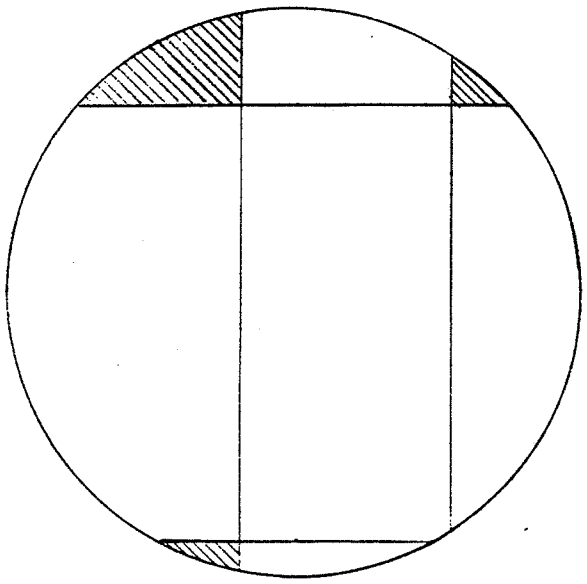

Figure 2.5 Shaded Areas Are Added to Circle Area

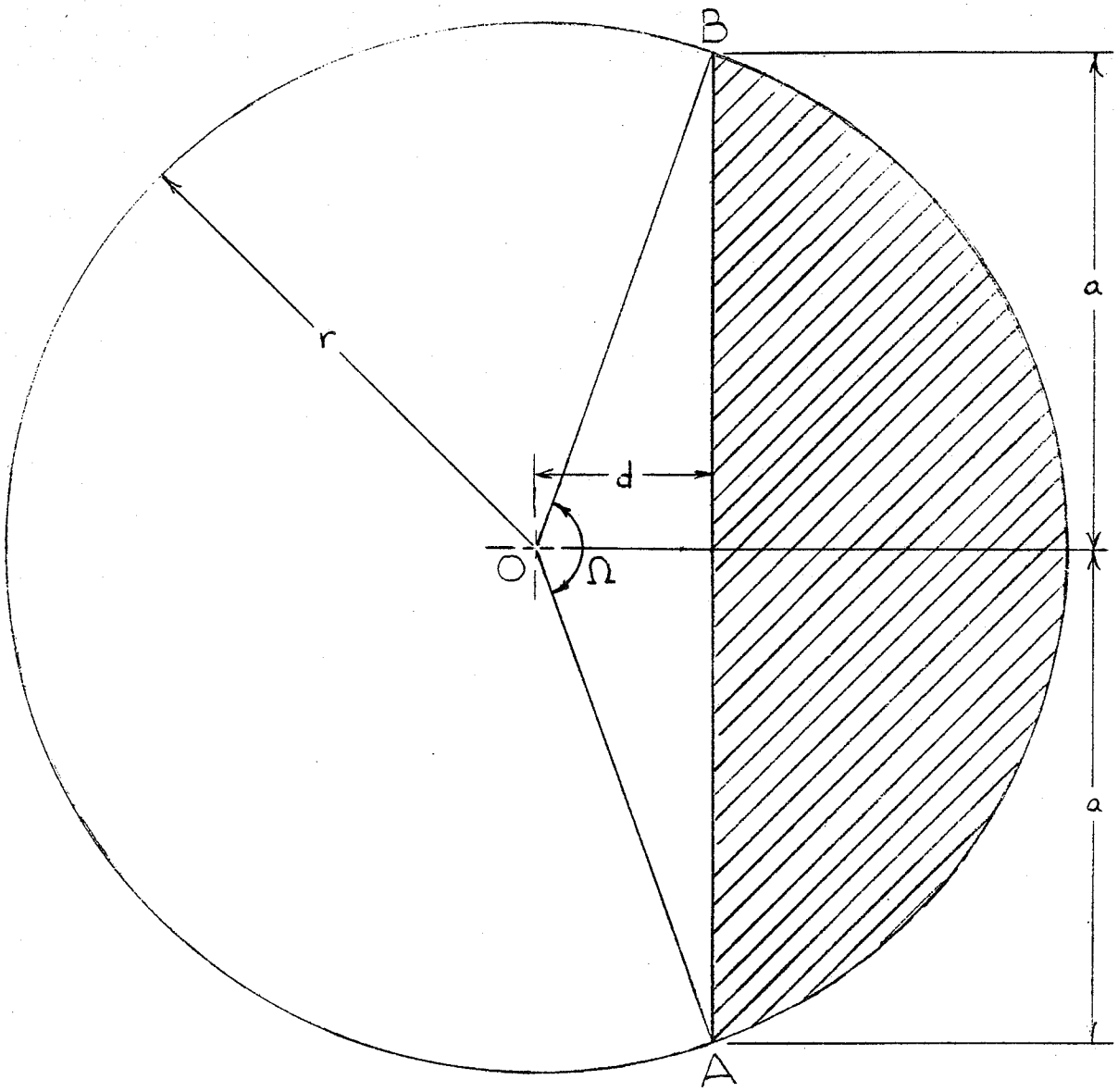

Figure 2.6 Geometry for Calculating Areas to be Subtracted from the Circle Area

$$\Omega = 2\tan^{-1}\left(\frac{\sqrt{r^2 - d^2}}{d}\right). \tag{2.30}$$

Thus, the total area can be expressed as

$$A = r^2 \tan^{-1}\left(\frac{\sqrt{r^2 - d^2}}{d}\right) - d\sqrt{r^2 - d^2}\ . \tag{2.31}$$

The inverse tangent function used in the above equations needs to be a two argument arctangent function when implemented on a computer so that the proper sign is used. This method gives the correct area even for negative values of d.

The areas to be added back onto the total area must be calculated from the same given variables as the areas subtracted from the total. The geometry is shown in Fig. 2.7 and the area of interest is defined by an arc and two lines intersecting at a right angle. The two possible ways of calculating the area are by finding the area of triangle ABC and adding the area defined by chord BC and arc BC, or by finding the area of sector COB and subtracting the areas of triangles AOC and AOB. Since both ways yield expressions of similar complexity, only the first method will be examined. The area needs to be found in terms of r, d_1, and d_2, but the intermediate variables f_1, f_2, s, and d will be defined first.

$$f_1 = \sqrt{r^2 - d_2^2} - d_1 \tag{2.32}$$

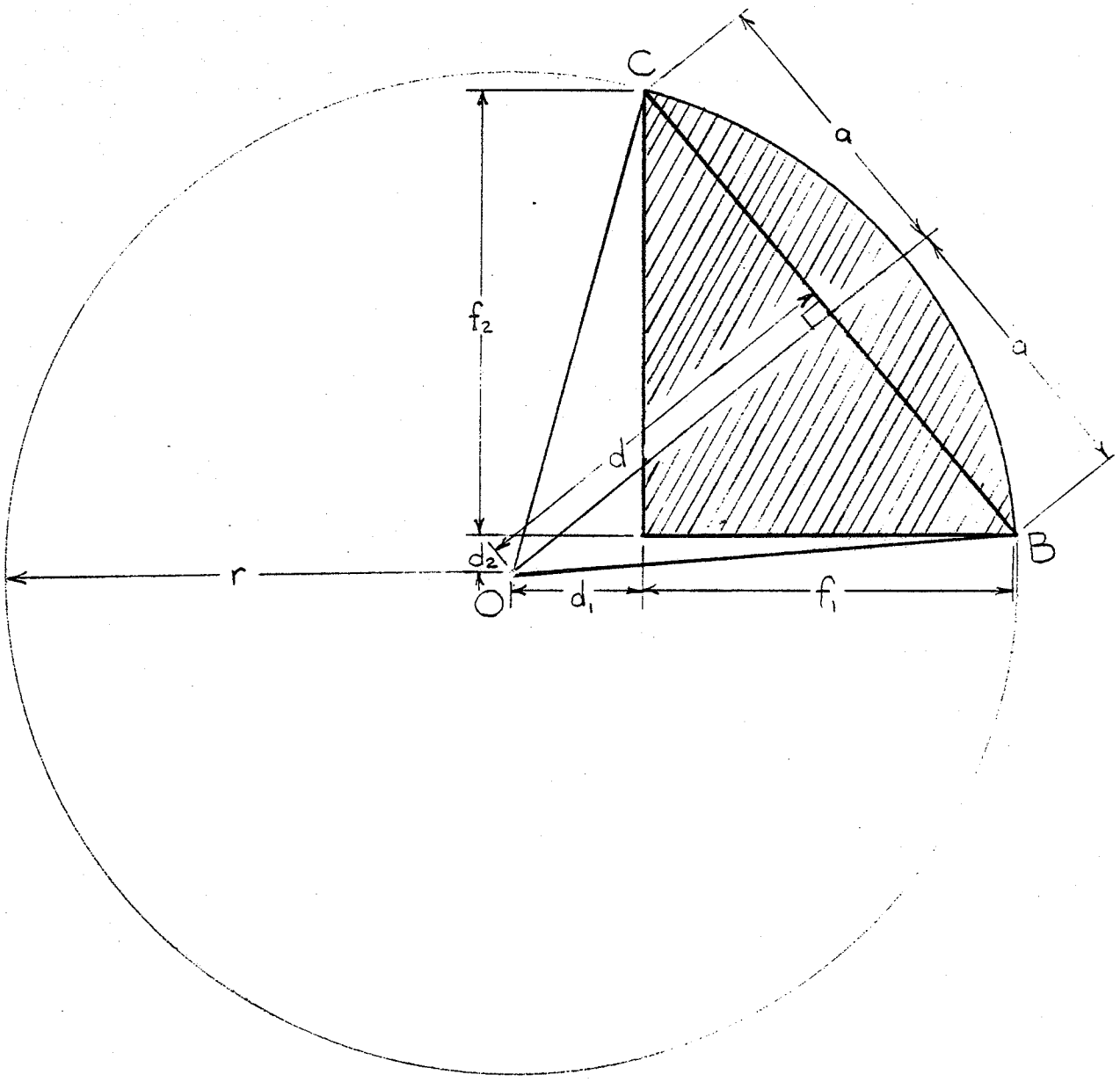

Figure 2.7 Geometry for Calculating Areas to be Added to the Circle Area

$$f_1 = \sqrt{r^2 - d_1^2} - d_2 \tag{2.33}$$

$$a = \frac{1}{2}\sqrt{f_1^2 + f_2^2} \tag{2.34}$$

$$d = \sqrt{r^2 - a^2} \quad . \tag{2.35}$$

The area can be expressed using these variables as

$$A = \frac{1}{2} f_1 f_2 + r^2 \tan^{-1}\left(\frac{a}{d}\right) - ad \quad . \tag{2.36}$$

Combining Eqs. (2.32) to (2.36) yields the area of Fig. 2.7 in terms of the given variables. Using these approaches to calculate the areas defined in Figs. 2.6 and 2.7, the calculation of the intersection of a circular area and a rectangular area may be completed.

The area of intersection formed by two concentric circles and a rectangle can be used to determine an area which is approximately equidistant from the field point for the entire source. The expression $s\Delta s/r$ defines the range in r for that area. The maximum distance error is $\Delta r/2$ for any point of an area ΔA. The limits for s, s_{min} and s_{max}, are found easily as s_{max} is always the distance from the projection of the field point on the x - y plane to the farthest corner of the element and s_{min} is (1) zero if the field point is within the x and y ranges of the element, (2) the distance from the field point projection to the

closest side of the element if the field point is within only the x or y range of the element, or (3) the distance from the field point projection to the nearest corner if the field point is not in the x or y range of the element.

This equidistant area method is best suited for source geometries where the equidistant areas are large, such as for the case of large unfocused planar transducers. Because of the narrow widths of linear phased array elements, dividing each element into equidistant areas produces many small areas and does not justify the complex computation used to determine each area. The effect of these approximations on field point pressure error is difficult to determine. Thus, for the array transducers of interest in this study, this method does not appear to be the best choice.

2.1.3 Point Radiator Method

One of the most straightforward methods that may be used to calculate the field involves representing the source by a large number of point radiators. This method is used for nearfield calculations and has been used to describe the field for circular piston sources [Zemanek, 1970]. The method is implemented by dividing the source into incremental areas that are small enough that the field produced by each can be approximated as that due to a point source placed at the center of the incremental area with an amplitude proportional to the size of the incremental area. This representation can be used only if the dimensions of the incremental areas are small compared to a wavelength. The integral over the surface (Eq. (2.4)) then becomes a summation over the surface

$$p_o = \frac{j\rho ck\Delta A}{2\pi} \sum_{\text{surface}} u(x_o,y_o)\frac{e^{-(\alpha+jk)r}}{r} \qquad (2.37)$$

where the incremental area $\Delta A = \Delta h \Delta w$ is used with Δh and Δw chosen to be much less than a wavelength.

If this method is used to find the pressure for a set of points in a constant z plane where the field points have the same x and y locations as the equally spaced points used to represent the array, and if the number of points is equal to a power of two in both the x and y directions, then this method would be equivalent to finding the field using a two dimensional linear convolution as described in Section 2.1.1 dealing with the Fourier transform. The advantages of the point radiator method over the linear convolution technique are evident when the constraints of the linear convolution are examined: (1) the points used to represent the array have to be spaced evenly giving many zero points in the space between elements, (2) the field points need to be spaced the same as the sample points, (3) a complete set of points in a constant z plane need to be evaluated, and (4) if an FFT is used to implement the linear convolution then the number of points needs to be an integer power of two.

For an accuracy equivalent to using the Fourier transform, the point radiators must be separated by one sixth of a wavelength, the same sampling frequency as used for the Fourier transform method. The point radiator method is most advantageous when the field is evaluated as a function of z, and for examining

an array having large spacings between elements as with a nonuniformly spaced array.

2.1.4 Rectangular Radiator Method

The phased array can also be represented by a number of subelements that are too large to be represented as point sources. The total pressure p_o at a point in the field is then the sum of the pressure contributed from each subelement as shown in the following relation

$$p_o = \frac{j\rho ck}{2\pi} \sum_{n=1}^{N} u_n \iint_{\Delta A} \frac{e^{-(\alpha+jk)r}}{r} dx_o dy_o \tag{2.38}$$

where N is the number of subelements of size $\Delta A = \Delta h \Delta w$ and u_n is the complex surface velocity for subelement n. The subelements are chosen so that each subelement represents part of only one element and does not contain any of the space between elements. The center of subelement n is denoted by (x_n, y_n) to simplify the analysis that follows. To simplify the integration, a coordinate system in x_o and y_o with its origin centered on the subelement is defined as shown in Fig. 2.8 . Applying this to Eq. (2.38) yields

$$p_o = \frac{j\rho ck}{2\pi} \sum_{n=1}^{N} u_n \int_{-\frac{\Delta h}{2}}^{\frac{\Delta h}{2}} \int_{-\frac{\Delta h}{2}}^{\frac{\Delta w}{2}} \frac{e^{-(\alpha+jk)r}}{r} dx_o dy_o \tag{2.39}$$

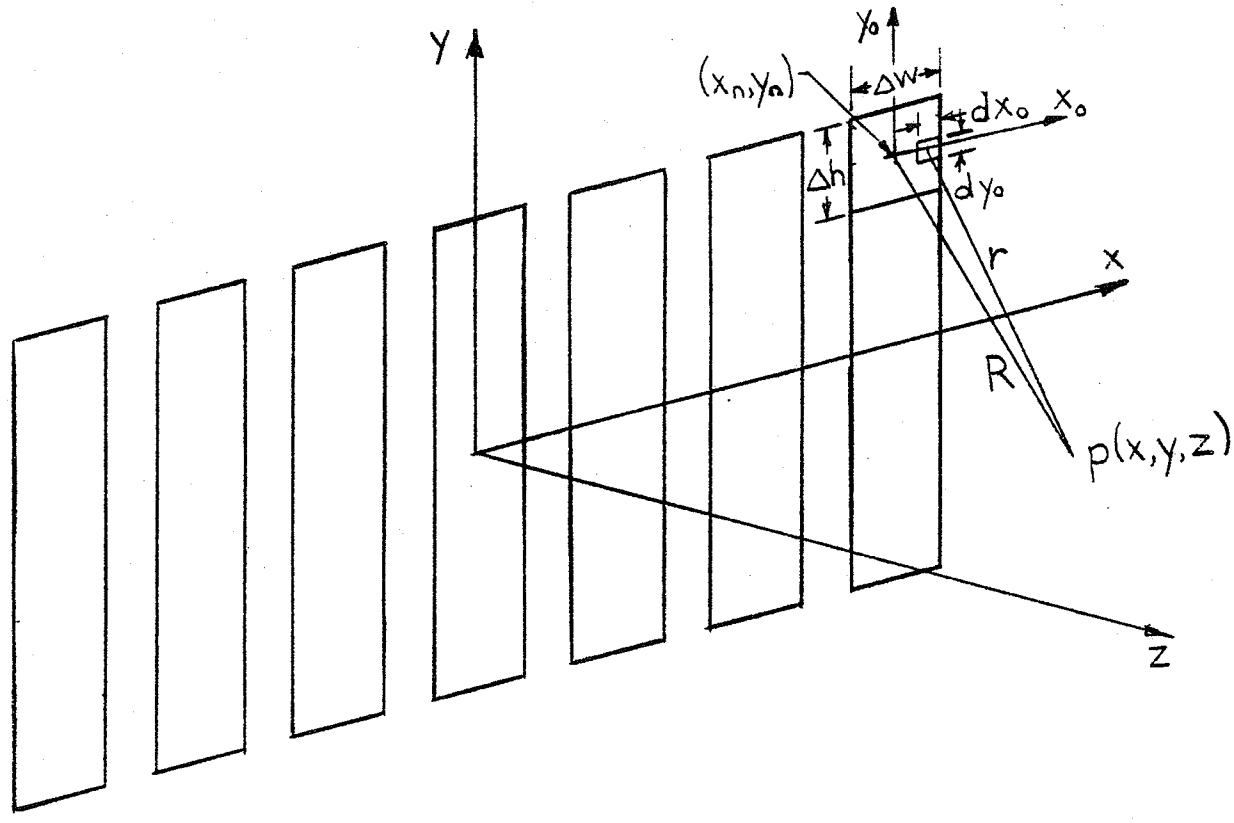

Figure 2.8 Geometry for Rectangular Radiation Method

where

$$r = \sqrt{z^2 + (x-x_n-x_o)^2 + (y-y_n-y_o)^2} \quad . \tag{2.40}$$

By choosing Δh and Δw to be small, the distance to the field point is made much greater than the dimensions of the source and the Fraunhofer approximations can be applied. The variables x' and y' are then defined as $x' = x - x_n$ and $y' = y - y_n$ for application of the approximation. Using Eq. (2.19) with x' and y' replacing x and y, the approximation $1/r \approx 1/R$, and substituting into Eq. (2.39) gives

$$p_o = \frac{j\rho ck}{2\pi} \sum_{n=1}^{N} \frac{u_n}{R} e^{-(\alpha+jk)R} \int_{-\frac{\Delta w}{2}}^{\frac{\Delta w}{2}} e^{\frac{jkx'x_o}{R}} dx_o \int_{-\frac{\Delta h}{2}}^{\frac{\Delta h}{2}} e^{\frac{jky'y_o}{R}} dy_o \tag{2.41}$$

where

$$R = \sqrt{z^2 + x'^2 + y'^2} \quad . \tag{2.42}$$

Integrating and simplifying Eq. (2.41) gives

$$p_o = \frac{j\rho ck\Delta A}{2\pi} \sum_{n=1}^{N} \frac{u_n}{R} e^{-(\alpha+jk)R} \operatorname{sinc}\left(\frac{kx'\Delta w}{2R}\right) \operatorname{sinc}\left(\frac{ky'\Delta h}{2R}\right) \quad . \tag{2.43}$$

Equation (2.43) is in a form that can be readily evaluated using a computer. Due to the approximation resulting from the use of Eq. (2.19), Eq. (2.43) is accurate only when $kx_o^2/2R + ky_o^2/2R$ is small compared to π and when $1/r \approx 1/R$. Since the maximum values of x_o and y_o are $\Delta w/2$ and $\Delta h/2$, respectively, these conditions can be expressed as $k\Delta w^2/8R + k\Delta h^2/8R$ small compared to π and $1/r \approx 1/R$. Choosing

$k\Delta w^2/8R + h^2/8R$ small ensures that $1/r \sim 1/R$ so that only one condition is necessary. The condition that $\pi >> k\Delta w^2/8R$ can be rewritten as $R >> k(\Delta w/2)^2/2\pi$, which is equivalent to the provision that the field point be in the farfield for an element dimension Δw. Since z is less than R, an equivalent condition is $z >> k(\Delta w/2)^2/2\pi$. A constant C can be defined and given a sufficiently large value such that the above condition is given by the following relation.

$$\Delta h, \Delta w \leq \sqrt{\frac{C 8\pi z}{k}} \quad . \tag{2.44}$$

The inequality sign is used so that Δw or Δh may be chosen to be smaller than the value an equality would yield such that the exact area of each element can be represented.

As the distance from the array becomes greater, the constraint on the size of the subelements is relaxed until the limiting case is reached where z is so large that $\Delta w = w$ and $\Delta h = h$. For very large z, the farfield expression is

$$p_o = \frac{j\rho ckhw}{2\pi} \sum_{n=1}^{N} u_n e^{-(\alpha+jk)R} \operatorname{sinc}\left(\frac{k(x-x_n)w}{2R}\right) \operatorname{sinc}\left(\frac{k(y-y_n)h}{2R}\right) \tag{2.45}$$

which is valid for $R >> kw^2/8\pi$ and $R >> kh^2/8\pi$. This illustrates that the rectangular radiator method is well suited for a wide range of field point locations and element sizes and that it will minimize calculation time if it is implemented to use the largest subelement size that will maintain the desired accuracy.

2.1.5 Rectangular Radiator Approximation Method

A comparison of the expressions for the point radiator method

(Eq. (2.37)) and the rectangular radiator method (Eq. (2.43)) shows that the difference is the directivity term $\mathrm{sinc}(kx'\Delta w/2R)\mathrm{sinc}(ky'\Delta w/2R)$ included in the latter. Since the calculation of the pressure does not require the full accuracy of the sine function in the evaluation of the sinc function, an approximation for the sinc function is possible. Four of the forms that could be used for an approximation are (1) power series, (2) Chebyshev polynomial, (3) continued fraction and (4) rational function [Froberg, 1969]. The power series

$$\mathrm{sinc}(x) = 1 - \frac{x^2}{3!} + \frac{x^4}{5!} - \frac{x^6}{7!} + \frac{x^8}{9!} - \ldots \tag{2.46}$$

and the rational function

$$\mathrm{sinc}(x) = \frac{1 - 0.133563936x^2 + 0.0032811761x^4}{1 + 0.0331027317x^2 + 0.0004649838x^4} \tag{2.47}$$

are examined briefly. The approximations are implemented by replacing the directivity term in Eq. (2.43) with the appropriate approximation.

The number of terms used in the power series approximation can be selected to control the range of the argument of the sinc function for which acceptable accuracy is obtained. Using only the first term in the power series expansion gives a directivity term equal to one and is equivalent to using the point radiator method of Eq. (2.37). Using this approximation the argument of the sinc function must be less than 0.55 in order to limit the maximum error to five percent. Examination of the argument of the sinc function reveals that its largest possible value occurs when

$x' = R$. Restricting the sinc function argument to be less than 0.55 for the largest possible argument yields

$$\frac{k\Delta w}{2} < .55 \quad . \tag{2.48}$$

Substituting $\lambda = 2\pi/k$ gives

$$\Delta w < \frac{1}{5.7}\lambda \tag{2.49}$$

which supports the choice of one sixth of a wave length spacing used for the point radiator method.

Since for a given amount of computation, the rational function expression is accurate over a larger range than the power series expansion [Froberg, 1969], a multiple term rational function was examined. Equation (2.47) is accurate to within five percent for argument magnitudes less than four so that using the reasoning applied to the development of Eq. (2.49) the condition

$$\Delta w < 1.2\,\lambda \tag{2.50}$$

is reached. However, grating lobes appear when equally spaced elements are wider than one wavelength, so element widths have been kept below a wavelength for this investigation. Thus, the rational function approximation or a power series expansion with a sufficient number of terms can be used for evaluation of the x dependent sinc function. To use either approximation for the y dependent sinc function, Δh would have to be chosen to satify both Eq. (2.44) and the inequality applied to Δw above. The rectangular radiator approximation method uses the same approach as the rectangular radiator method, but it is more efficient because of its additional approximations. However, these

additional approximations result in larger errors so that this method must be used with caution.

2.2 Results

Programs were written to implement each of the field calculation methods described in Section 2.1. All of the programs were written in Fortran except for a pre-existing FFT routine which used assembly language. Listings of the programs as they were implemented on the Bioacoustics Research Laboratory's Perkin Elmer 7/32 computer form the Appendices.

Results of the programs were compared for a sixteen element linear phased array. The array was chosen to have elements 2.5 mm wide by 50.0 mm high with 3.0 mm distance between adjacent element centers and to have an operating frequency of 600 kHz. The phases for the array elements were specified to produce a focus at an x distance of 3 cm from the center of the array and a z distance 10 cm from the array. Figures 2.9 through 2.13 show the field intensity, which is proportional to the square of the pressure, as a function of x at z = 10 cm for each of the calculation methods. Figures 2.9 through 2.13 show the intensity obtained using the the Fraunhofer approximation, the point raditator, the equidistant area, the rectangular radiator, and the rectangular radiator approximation methods, respectively. No results were obtained for the Fourier Transform method without approximations or the Fresnel approximation method because the array size was too large to be represented in the core memory of the Perkin Elmer 7/32 computer. The difference in the result produced using the Fraunhofer approximations shows the limitations encountered when using simple

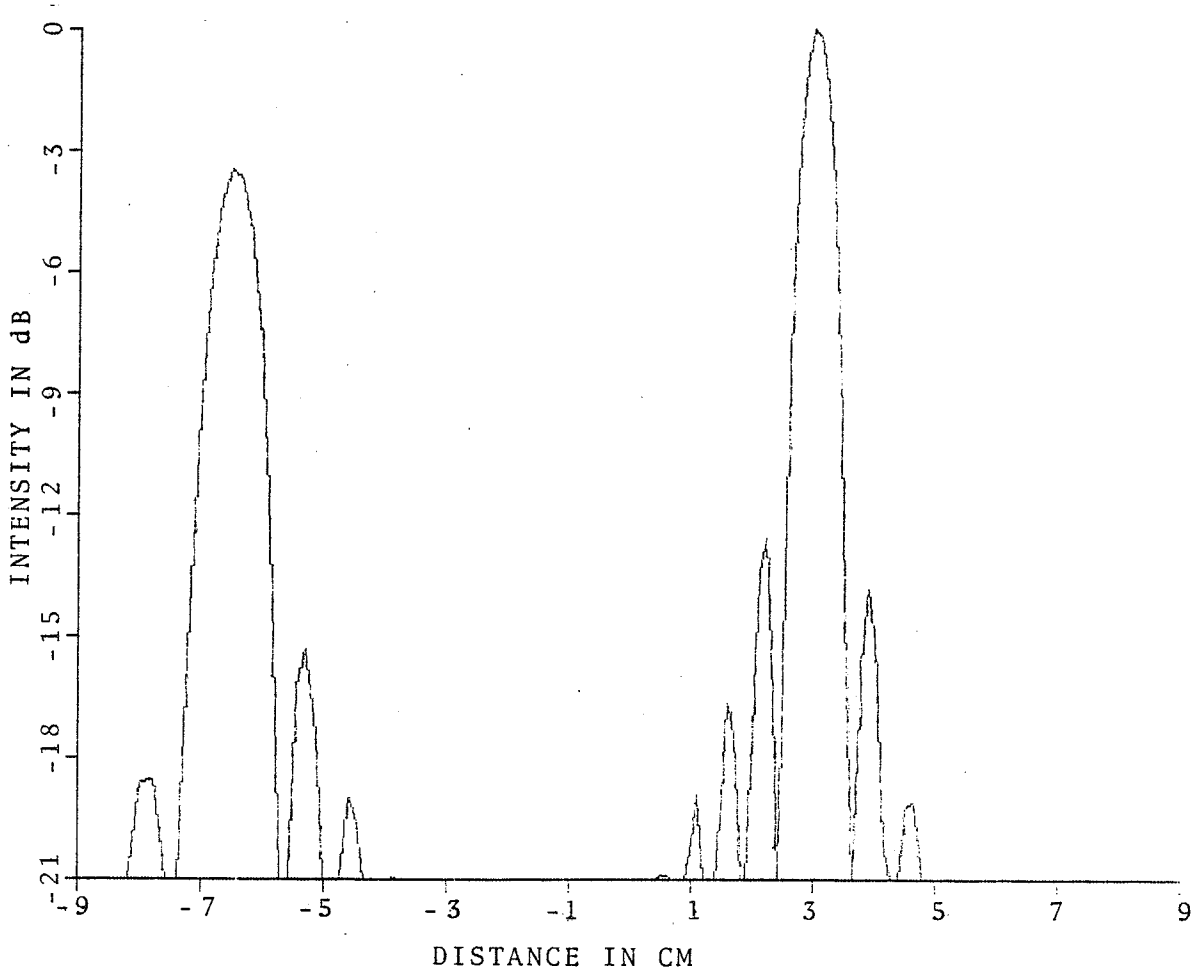

Figure 2.9 Field Profile Calculated Using Fraunhofer Approximation Method. Run Time = 6"

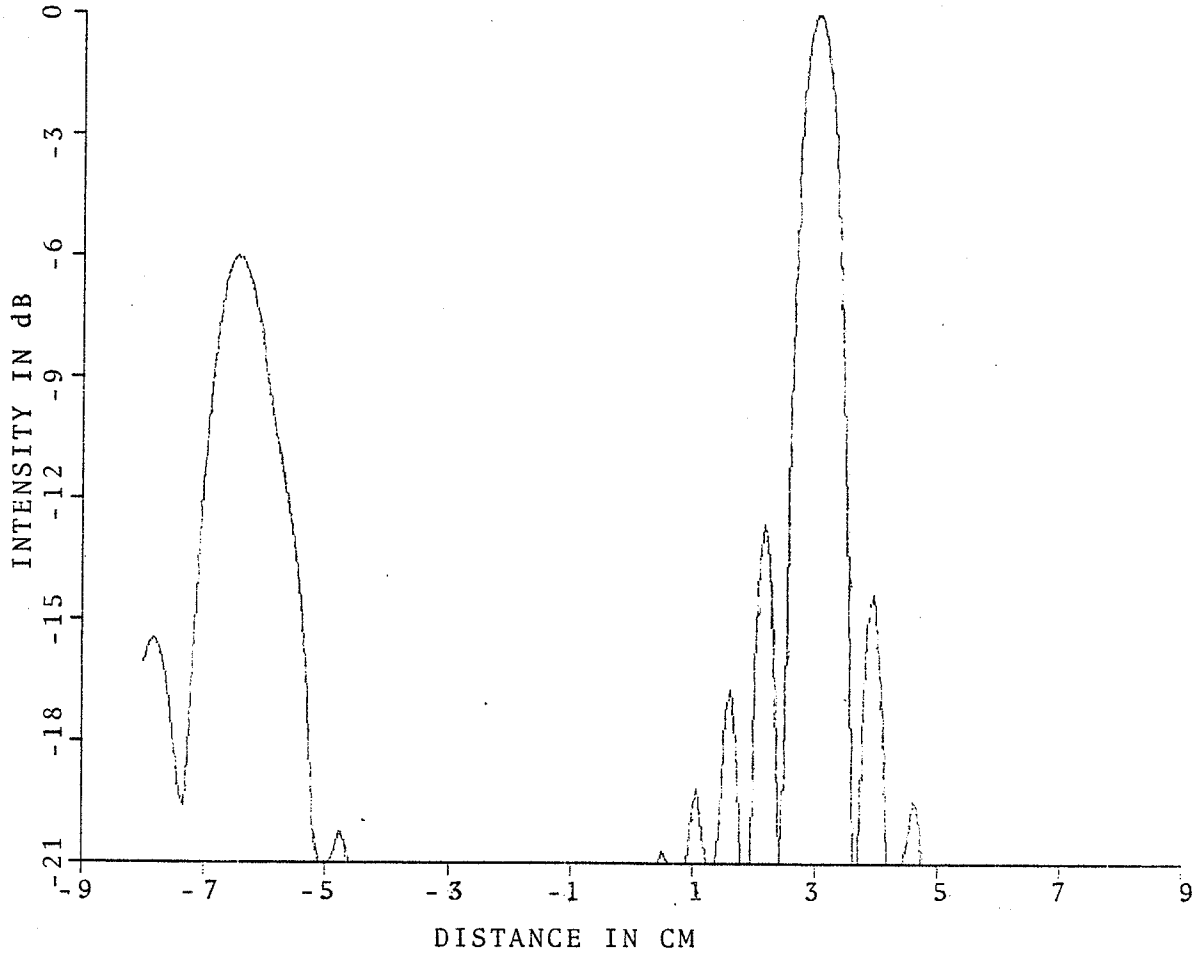

Figure 2.10 Field Profile Calculated Using Point Radiator Method.
Run Time = 38'34"

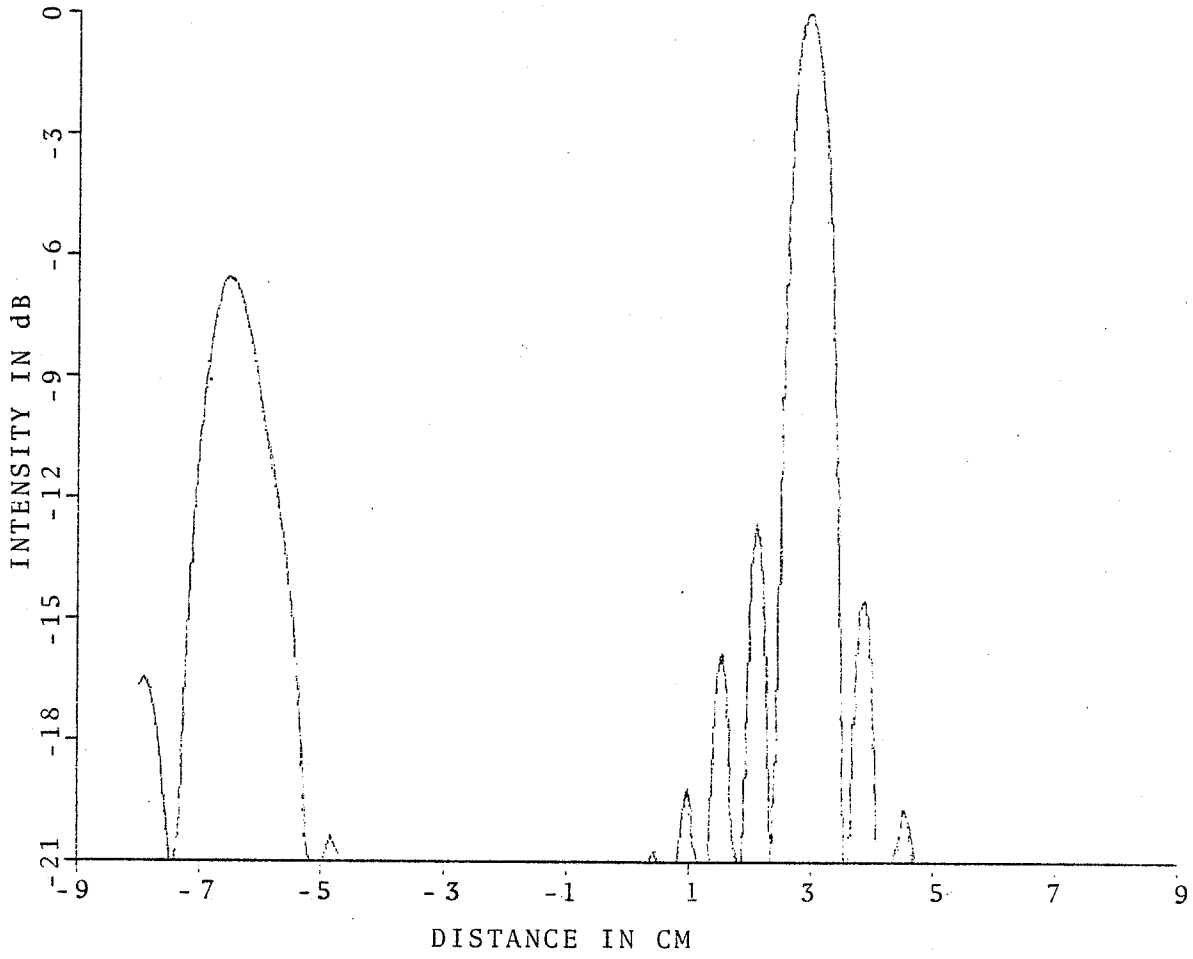

Figure 2.11 Field Profile Calculated Using Equidistant Area Method. Run Time = 5'28"

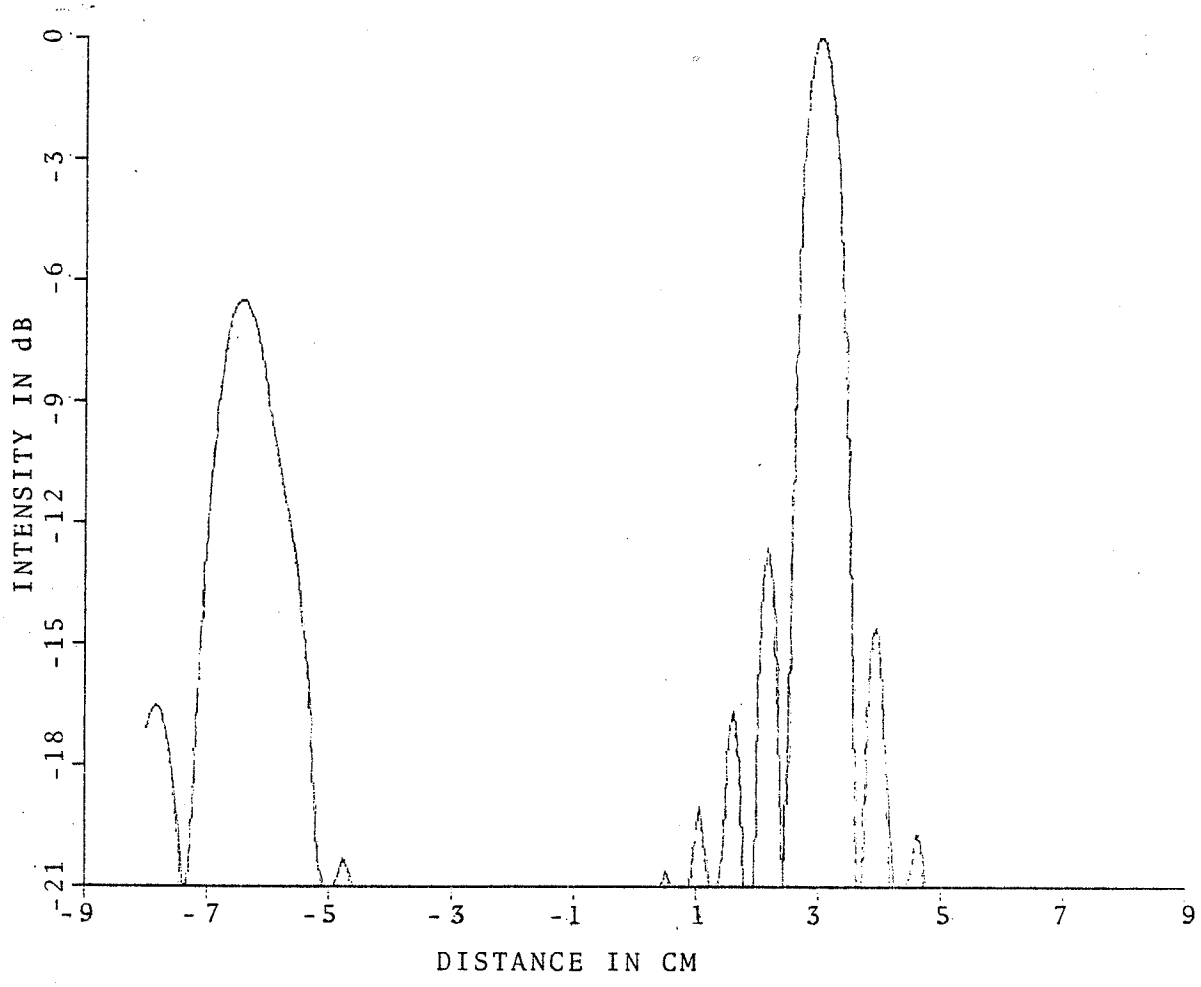

Figure 2.12 Field Profile Calculated Using Rectangular Radiator Method. Run Time = 46"

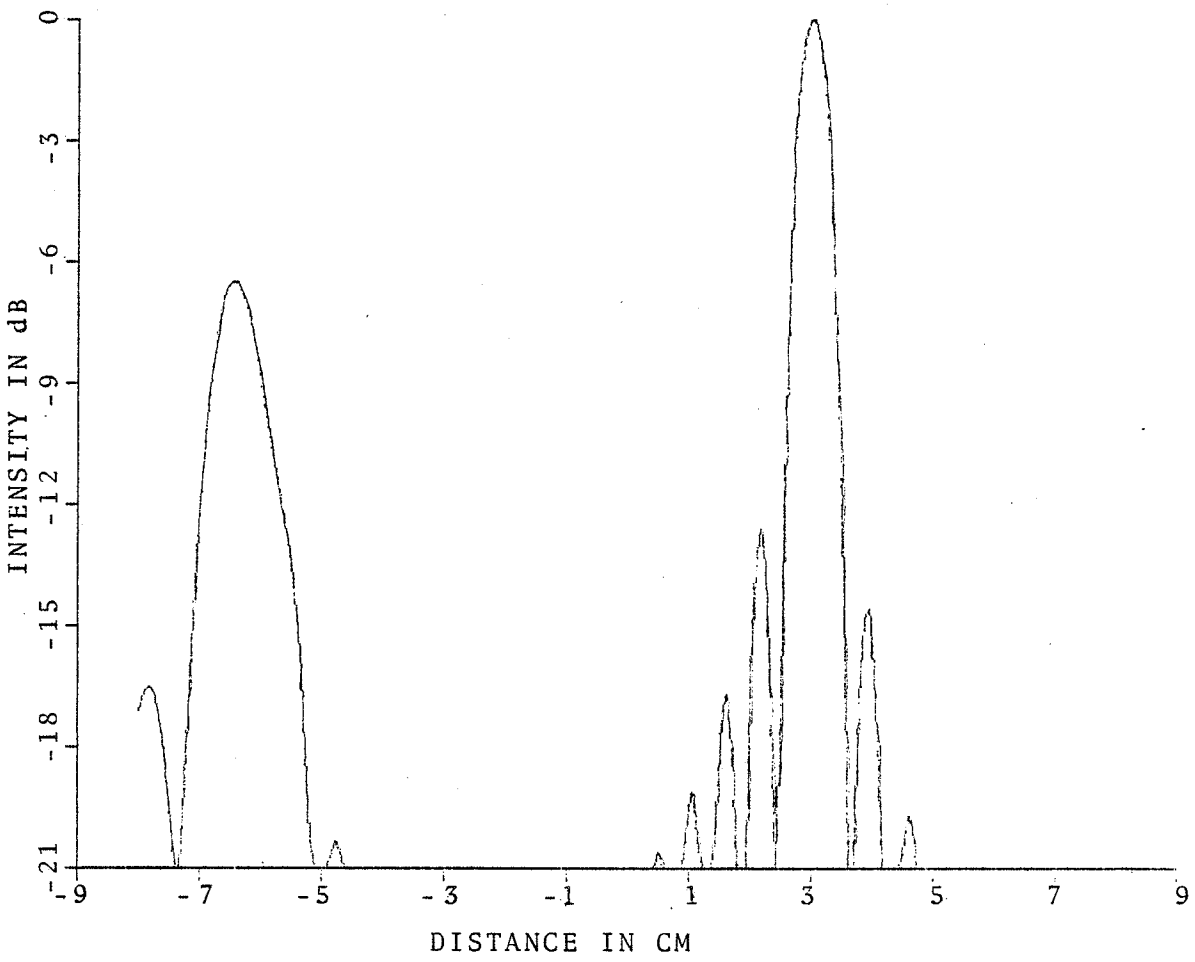

Figure 2.13 Field Profile Calculated Using Rectangular Radiator Approximation Method. Run Time = 40"

approximating techniques.

The time for computing each field profile is noted in the figure captions. The computation time varies significantly for methods which yield similar accuracy. It is readily seen that the rectangular radiator method gives accurate results with a minimum of calculation time. The determination of an efficient method for calculating the field produced by an array was necessary because the field calculation program will be used extensively to test new design concepts during the development of a phased array for hyperthermia.

CHAPTER 3

CALCULATION OF HEATING

The goal of an ultrasonic hyperthermia array is to produce localized heating. Thus, it is desirable to determine the heat generation rate as a function of space and its relation to the power radiated. Since the power radiated from an ultrasonic transducer is expected to be a limiting variable for hyperthermic treatment, the relationship between power radiated and heat generation rate will give the maximum possible heating for a given array configuration.

The relationship between heating per unit volume and pressure [Nyborg, 1981] is expressible as

$$\langle q_v \rangle = \alpha p_o^2/\rho c \qquad (3.1)$$

where α, ρ, and c are the attenuation, density, and sound velocity, respectively, of the medium. The pressure amplitude p_o is given by

$$p_o = \left| \frac{j\rho ck}{2\pi} \int_s \frac{u_o e^{j\beta}}{r} e^{-(\alpha+jk)r} \, ds \right| \qquad (3.2)$$

where u_o and β are the magnitude and phase, respectively, of the surface velocity. Equation (3.1) is valid for a single frequency field where the effects of shear viscosity can be ignored. Thus, the heating rate at any location can be calculated by using one of the methods described in Section 2.1 to determine the pressure amplitude and then applying Eq. (3.1).

Alternately, the heat generation rate can be expressed in terms of the total power radiated by finding the relationship between the pressure and the radiated power. Defining W as the total average power radiated by an element and I as the average intensity gives W = Ihw. The average power radiated over a complete cycle can be expressed as

$$W = \frac{1}{T} \int_0^T \mathrm{Re}\{f_s\}\, \mathrm{Re}\{u_o e^{j\omega t}\}\, dt \qquad (3.3)$$

where f_s is the force of the medium on the radiating surface, u is the magnitude of the surface velocity, and T is the length of one period.

At this point, it is necessary to introduce the radiation impedance which is defined as the ratio of the force produced by the element to the surface velocity of the element. Assuming that each element can be represented as a rigid source in rectilinear motion, the radiation impedance is

$$Z_r = \frac{f_s}{u_o e^{j\omega t}} \qquad (3.4)$$

which can be separated into its real and imaginary components as

$$Z_r = R_r + jX_r \quad . \qquad (3.5)$$

The radiation impedance for rectangular sources has been calculated by several investigators [Swenson and Johnson, 1951; Arase, 1964; Lindemann, 1971] and tabulated [Burnett and Soroka, 1972]. The tables generated by Burnett illustrate that for rectangular sources with sizes and length to width ratios like

those of linear array elements (.5 to 1 wavelength wide and length to width ratios from 10 to 50), the real component of the radiation impedance is dominant and approximately equal to ρchw.

Rearranging Eq. (3.4) to solve for f_s and substituting into Eq. (3.3) gives

$$W = \frac{1}{T} \int_o^T \mathrm{Re}\left\{ Z_r u_o e^{j\omega t} \right\} \mathrm{Re}\left\{ u_o e^{j\omega t} \right\} dt \quad . \tag{3.6}$$

Using Eq. (3.5) to replace Z_r yields

$$W = \frac{1}{T} \int_o^T \mathrm{Re}\{(R_r + jX_r)\, u_o(\cos\omega t + j\sin\omega t)\}\, u_o \cos\omega t\, dt \quad . \tag{3.7}$$

Further simplification and integration give

$$W = \frac{1}{2}\, u_o^2\, R_r \quad . \tag{3.8}$$

Substituting ρchw for R_r and Ihw for W in Eq. (3.8) and solving for u_o yields

$$u_o = \sqrt{\frac{2I}{\rho c}} \quad . \tag{3.9}$$

The complex surface velocity is then

$$u = u_o e^{j\beta} = \sqrt{\frac{2I}{\rho c}}\; e^{j\beta} \quad . \tag{3.10}$$

This equation gives the surface velocity of an element, as used in Eq. (3.2), in terms of the average intensity emitted from the element. This allows the pressure and heat generation rate to be calculated for a given acoustic intensity at the element surface.

CHAPTER 4

DETERMINATION OF THE NUMBER OF BITS FOR PHASING

4.1 Theory

Since digitally programmable counters were chosen to control the phase of the signals applied to the elements of the array, the appropriate number of bits to be used in the counters needs to be determined. The choice of programmable counters allows each counter to be initialized to any count state, which determines the phase of the output. One full count corresponds to each cycle of the output frequency. Thus, for a full count of N, one output cycle results for each N input cycles and the phase can be adjusted in quantum steps of 360/N degrees. Clearly, as more bits are used N becomes larger, the phasing becomes more precise, and the focus better defined. A large number of bits means that a high clock rate (input frequency) is required and more complex circuitry is necessary to support the increased resolution, whereas a small number of bits makes implementation of the electronics simpler but may result in a degraded focus. A model was developed to determine the performance degradation due to quantization error so that the tradeoff between simplicity and performance could be examined.

The model provides the decrease in intensity at the focus for the average and worst case quantization error. For points in the field that are not near the focus, the quantization error will not affect the average intensity since the phases are essentially random. The worst case rise in intensity at these points is

calculated making certain assumptions about the distribution of the phases at these points.

The average degradation of intensity at the focus can be calculated easily since it is desired that the contributions from all of the elements have the same phase when they reach the focal point. Quantization to n bits quantizes the phases to $2\pi/2^n$ radians so that the greatest phase error possible is $\pi/2^n$ radians. For the average case, phase errors will be distributed uniformly from $-\pi/2^n$ to $\pi/2^n$ as shown in Fig. 4.1. The amplitude at the focal point due to such a phase distribution, normalized to unit amplitude for completely additive phasing, is

$$A = \frac{2^n}{2} \int_{-\pi/2^n}^{\pi/2^n} e^{j\beta}\, d\beta = \frac{2^n}{\pi} \sin\left(\frac{\pi}{2^n}\right) \quad . \tag{4.1}$$

The evaluation of this expression for different values of n is presented in Table 4.1. These values agree with those calculated for the electromagnetic case by Steinberg [Steinberg, 1976]. As expected, as n becomes large, the quantization error becomes less and the intensity approaches one.

The worst case quantization at the focus is when all the phases are at the maximum error, half with positive phase error and the other half with negative phase error. After quantization the phases are distributed as shown in Fig. 4.2. The amplitude for worst case quantization is

$$A = \frac{1}{2} e^{j\pi/2^n} + \frac{1}{2} e^{-j\pi/2^n} = \cos\left(\frac{\pi}{2^n}\right) \quad . \tag{4.2}$$

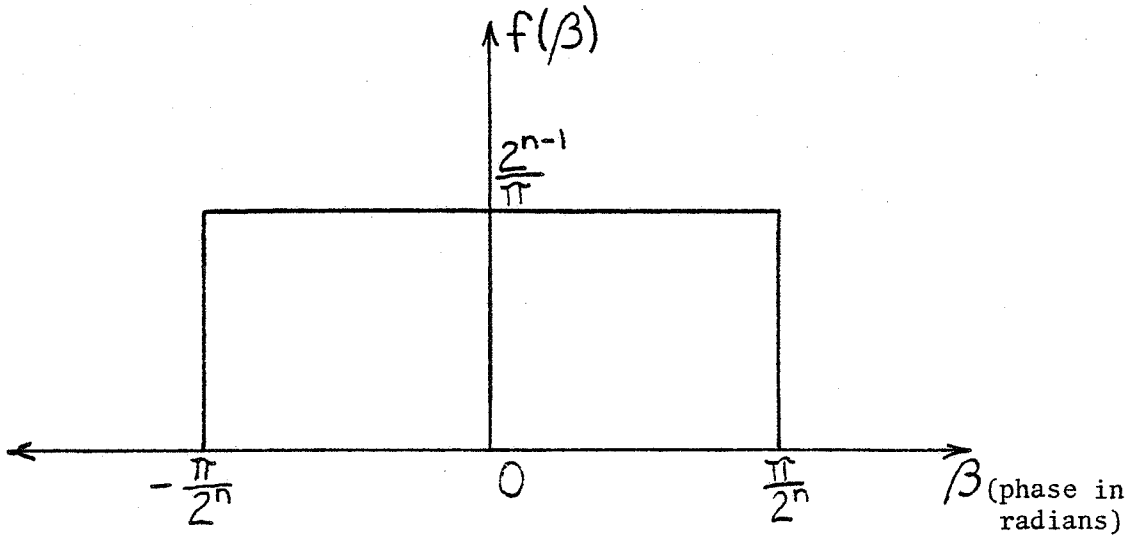

Figure 4.1 Phase Distribution for Average Case

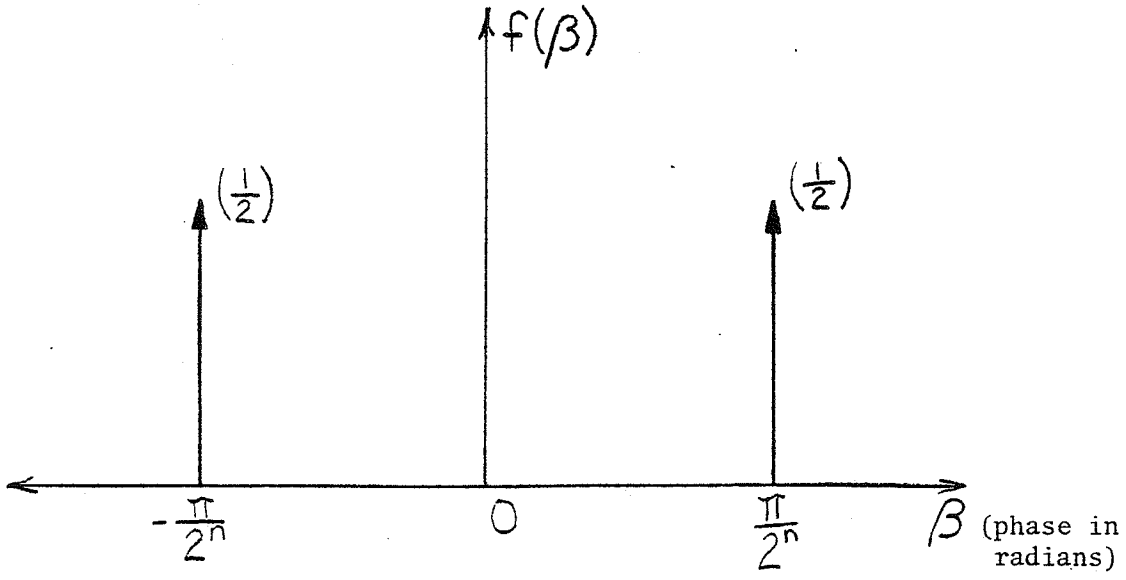

Figure 4.2 Phase Distribution for Worst Case

Table 4.1 Effect of Phase Quantization

Number of bits n	Maximum Phase Error (degrees)	Average Intensity Decrease at Focus Due to Quantization (dB)	Maximum Intensity Decrease at Focus Due to Quantization (dB)
1	90.0	3.922	infinite
2	45.0	0.912	3.010
3	22.5	0.224	0.688
4	11.25	0.0559	0.169
5	5.63	0.0140	0.0419
6	2.81	0.0035	0.0105
7	1.41	0.0009	0.0026
8	0.703	0.0002	0.0007

Table 4.1 also shows the intensity at the focus for worst case quantization. As is expected, the intensity at the focus is always less in the worst case than the average case.

The effect of quantization error on the intensity at points away from the focus (noise points) will now be examined. To represent a noise point, a phase distribution representative of an off focus point needs to be chosen. Three possible phase distributions to represent noise points are shown in Fig. 4.3. A model is sought that can be used to represent both low intensity and high intensity points. The parameters γ, σ, and Ω allow for variance of the noise point intensity for each of the distributions shown.

The range of intensity levels that can be represented by using the distribution of Fig. 4.3a was determined by finding the intensity level for a given γ. The normalized amplitude for such a distribution of phases is given by

$$A = \int_{-\pi}^{0} \left(\frac{1}{2\pi} + \gamma + \frac{2\gamma\beta}{\pi}\right) e^{j\beta} d\beta + \int_{0}^{\pi} \left(\frac{1}{2\pi} + \gamma - \frac{2\gamma\beta}{\pi}\right) e^{j\beta} d\beta \qquad (4.3)$$

which integrates to $8\gamma/\pi$. The maximum representable amplitude is for $\gamma=1/2\pi$, which gives an amplitude of 0.41 with a corresponding intensity of -7.84 dB. Since grating lobes can often peak above -3 dB and the noise points of greatest concern are those of high amplitude, this method does not have a sufficient range of intensity.

The Gaussian distribution of phase errors as shown in Fig. 4.3b has a normalized amplitude of

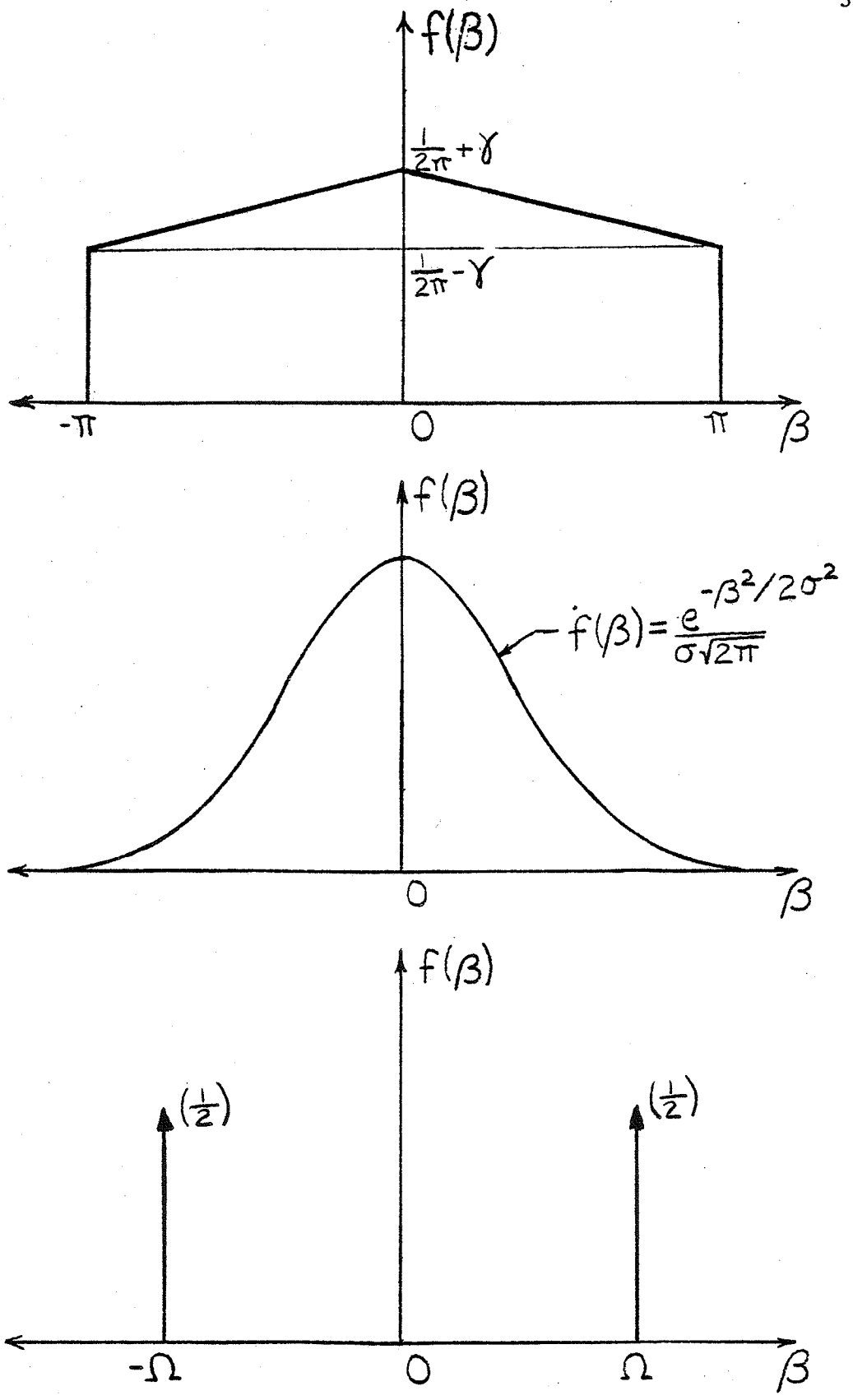

Figure 4.3 Phase Distributions for Noise Point Representation

$$A = \frac{1}{\sigma\sqrt{2\pi}} \int_{-\pi}^{\pi} e^{-\beta^2/2\sigma^2} e^{j\beta} d\beta \quad . \tag{4.4}$$

This expression truncates the extended portions of the curve, and for small σ (less than π) the limits can be changed to infinity without much effect. Changing the limits and integrating gives

$$A = \frac{\sqrt{2}}{\sigma\pi} \int_{0}^{\infty} e^{-\beta^2/2\sigma^2} \cos\beta d\beta = e^{-\sigma^2/2} \quad . \tag{4.5}$$

By the proper choice of σ, the amplitude can be set from zero to one, remembering that for large σ there is wraparound and the disribution becomes less Gaussian in shape.

For the Gaussian distribution of phase errors, the worst case quantization changes the distribution to look like Fig. 4.4. The amplitude of the noise after worst case quantization is

$$A = \frac{\sqrt{2}}{\sigma\pi} \int_{0}^{\frac{\pi}{2^n}} e^{-\frac{\beta^2}{2\sigma^2}} d\beta + \frac{1}{\sigma\sqrt{2\pi}} \left[\int_{-\infty}^{\frac{-\pi}{2^n}} e^{-\frac{\beta^2}{2\sigma^2}} e^{j(\beta + \frac{\pi}{2^n})} d\beta + \right. \tag{4.6}$$

$$\left. \int_{\frac{\pi}{2^n}}^{\infty} e^{-\frac{\beta^2}{2\sigma^2}} e^{j(\beta - \frac{\pi}{2^n})} d\beta \right] \quad .$$

The integrals of Eq. (4.6) can be simplified, but still must be evaluated numerically using a computer. The impetus for choosing a Gaussian distribution for a model is that for a random event sampled at random, the distribution approaches a Gaussian.

The modelling of the phases at a noise point as equivalent to two impulse functions of equal weighting is attractive because of

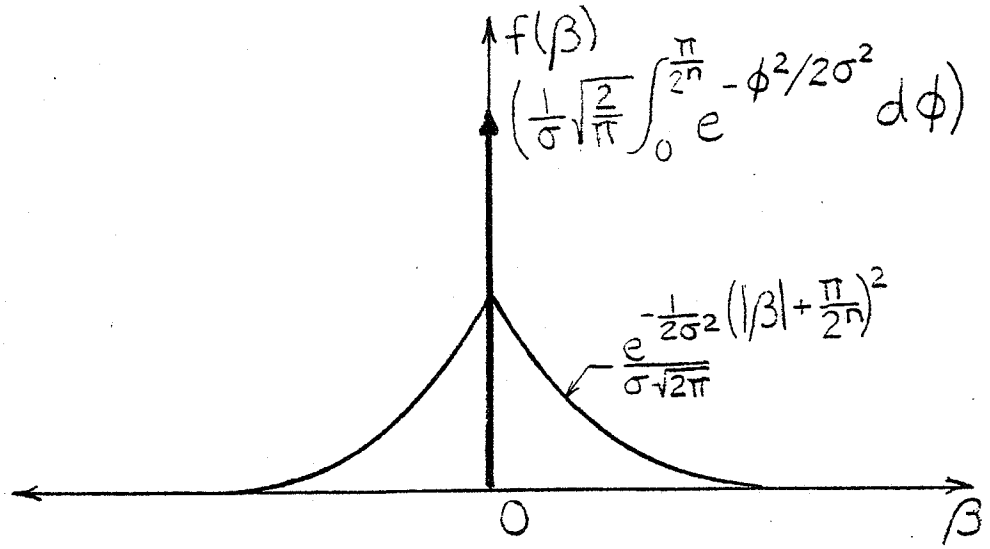

Figure 4.4 Worst Case Quantization of Gaussian Phase Distribution

the simplicity of the calculations involved. For two impulse functions with weightings of one half located at Ω and $-\Omega$ representing the phasing at the noise point, the resulting amplitude is simply $\cos(\Omega)$. Worst case quantization error brings the impulses closer together as shown in Fig. 4.5 and gives a resulting amplitude of

$$A = \begin{cases} 1 & \text{For } \Omega \leq \pi/2^n \\ \cos(\Omega - \pi/2^n) & \text{For } \Omega > \pi/2^n \end{cases} . \qquad (4.7)$$

A simple relation exists between the intensity in the unquantized signal and the angle Ω. Thus, for a given intensity for the unquantized signal, a calculation of the maximum possible intensity of the quantized signal can be made for a given number of bits assuming that the model used is representative of typical phasings.

4.2 Results

Comparisons of the results for a Gaussian phase distribution and those for a two impulse phase distribution show that the distributions are affected similarly by quantization errors. This similarity of reaction to phase errors leads to the conclusion that although the two impulse representation does not accurately represent the actual phase distribution at a noise point, it can be used as a model to predict the effect of phase on noise point amplitude.

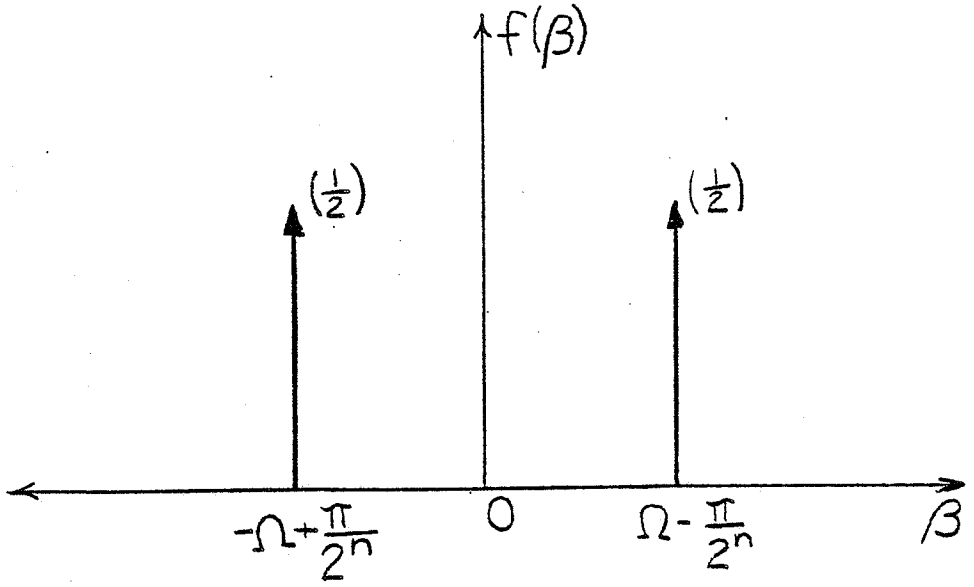

Figure 4.5 Worst Case Quantization of Impulse Phase Distribution

CHAPTER 5

USING PHASE SHIFTS TO REDUCE GRATING LOBES

5.1 Theory

The results of the intensity field plots show that the focal region is much more localized than necessary and that the grating lobe is the main hindrance to wider steering angles. The possibility of allowing some broadening of the focus to reduce the grating lobes is examined in this chapter. When a phasing scheme is chosen such that the contributions from all the elements do not add in phase at the focus, there is a lessening of the intensity at the focus. The tradeoff then becomes one of decreasing the intensity of the grating lobes more than it is decreased in the focal region.

The inspiration for this manipulation of phases comes from the two impulse phase distribution for modelling the phases at a noise point. For a given number of bits, the rise in the intensity for worst case quantization is more for a point with a lower initial intensity (Eq. (4.7)). Thus, when the same phase shift is added to two different points, the intensity at the point with the lower initial intensity will change more. If the phase shifts are made so that they reduce the intensity at a point on the grating lobe, that reduction will be greater than the intensity reduction at the focus so that the ratio of the focal intensity to the grating lobe intensity is increased and the grating lobe is reduced relative to the focal point. This reasoning is not dependent on the distribution of the phase errors at the noise point, but assumes that the phase shifts are made

such that the intensity is reduced at the noise point. However, this method cannot predict what will occur at points other than the focus and the point chosen to be reduced. The possible reduction in the grating lobe can be illustrated by Fig. 5.1. Figure 5.1 shows the intensity loss as a function of initial intensity level that occurs when phase shifts of five, ten, and twenty degrees are added to the two impulse phase distribution. The intensity level before adding the phase shifts is a function of the locations of the impulse functions. Twenty degrees is chosen as the maximum phase shift illustrated because above twenty degrees the intensity at the focus is lowered by over ten percent by the phasing which is too great a sacrifice of power.

5.2 Results

This method is implemented by phasing the array elements for a desired focus and then choosing an off focus point where the intensity level is to be lowered. The point would usually be chosen as a grating lobe peak, which could be located by using an exact field calculation or a farfield approximation. The relative phase of the pressure contributed from each element to the field at the chosen point is then calculated along with the total relative phase at the point. The phase contributed from an element is compared with the total phase and the phase of the driving signal is shifted by a fixed phase shift so that the difference between the contributed phase and the total phase is made larger. The magnitude of the fixed phase shift is dependent on the acceptable loss of power at the focus.

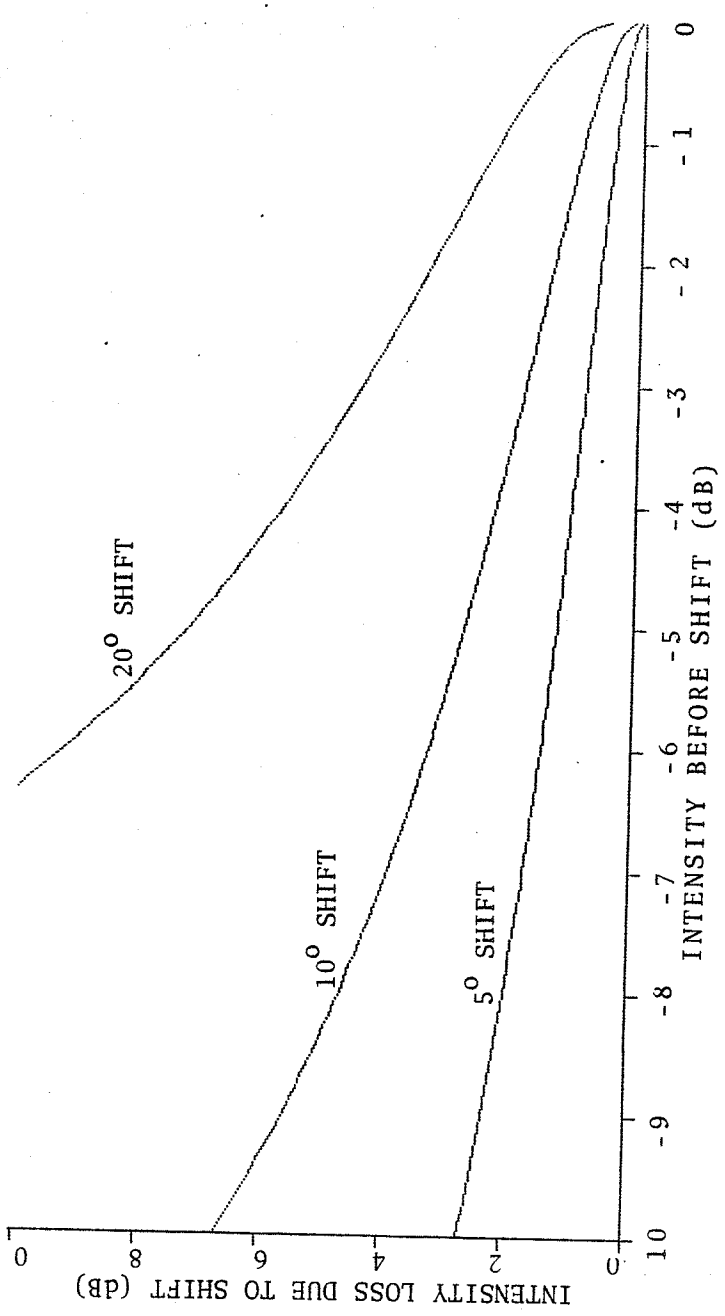

Figurge 5.1 Intensity Loss Due to Adding Phase Shifts of 5, 10, and 20 Degrees as a Function of Power Before Shift

The shift method was implemented for a sixteen element linear phased array. The array had elements 2.5 mm wide by 50.0 mm high with 3.0 mm distance between adjacent element centers. Figure 5.2 shows an intensity profile computed by specifying phases for the array elements that would produce a focus at an x distance of 3 cm from the center of the array and a z distance 10 cm from the array. The figure shows the field intensity as a function of x at z = 100 mm. The location of the grating lobe is at x = -6.5 cm in Fig. 5.2. The grating lobe amplitude was reduced by using phase shifts of twenty degrees. The necessary calculations of phases are shown in Table 5.1 and the resultant intensity distribution is shown in Fig. 5.3. Figures 5.2 and 5.3 can be directly compared to see the field changes resulting from adding phase shifts. The addition of phase shifts has lowered the intensity at the grating lobe maximum by 1 dB, which is only a small fraction of the 10 dB loss that would be predicted by using the graph of Fig. 5.1. This suggests that the two impulse phase distribution model is not sufficient for predicting the effect of phase shifts on grating lobe intensities.

A method of decreasing the grating lobe by using phase shifts has been demonstrated. Although the method works, the performance improvement does not justify the necessary calculations for finding which direction to apply the shift to each element.

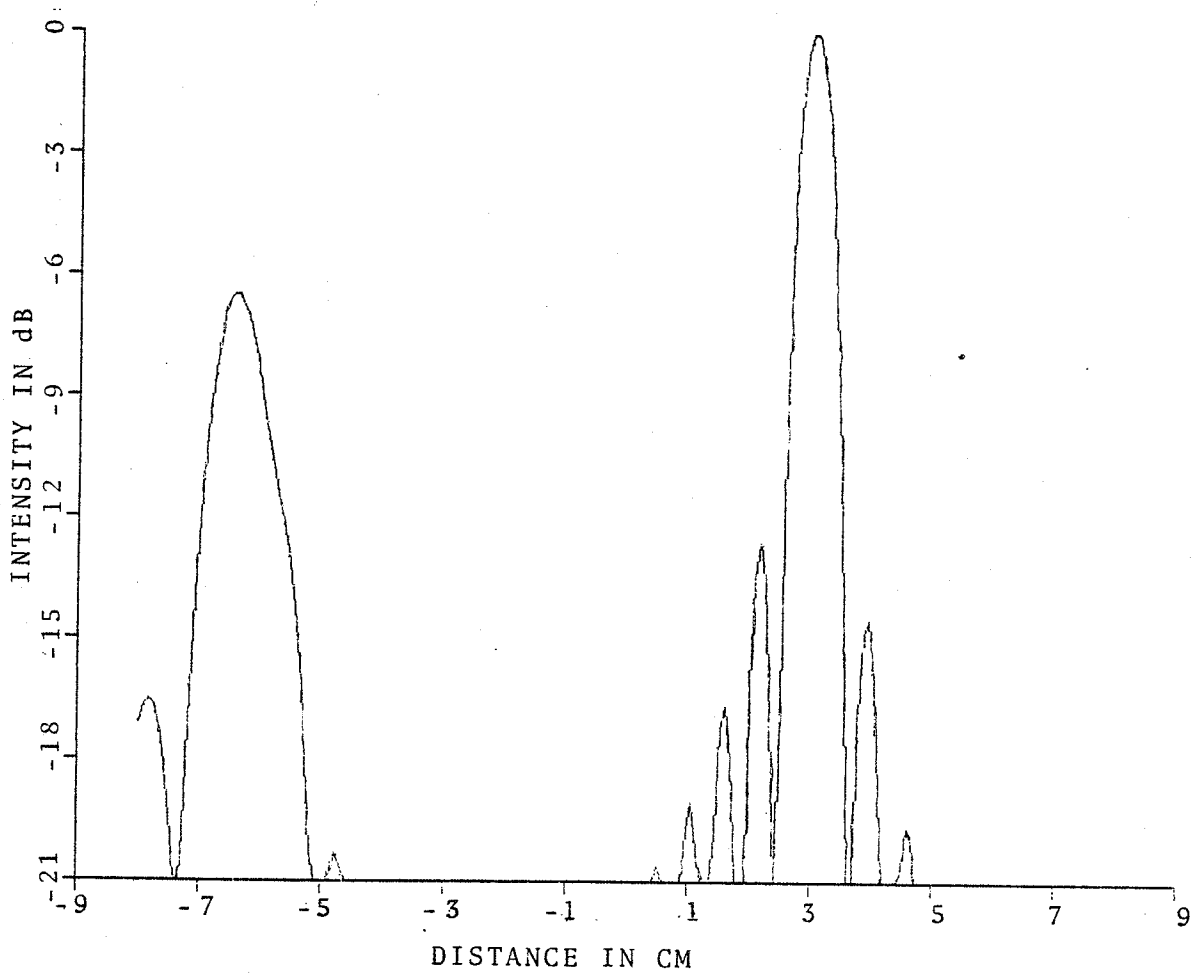

Figure 5.2 Intensity Profile without Shift

Table 5.1 Calculations Necessary for Phase Shifting (Phases in Degrees)

Element	X Coordinate of Element Center (mm)	Phasing on Element for Unshifted Focus	Phase at Grating Lobe for Unshifted Focus	Phase Shift to Reduce Grating Lobe	Phasing on Element After 20° Phase Shift
1	-22.5	149.83	316.16	+20	169.83
2	-19.5	313.58	304.36	+20	333.58
3	-16.5	126.65	292.16	+20	146.65
4	-13.5	309.39	280.24	+20	329.39
5	-10.5	142.12	269.26	-20	122.12
6	- 7.5	345.17	259.87	-20	325.17
7	- 4.5	198.85	252.73	-20	178.85
8	- 1.5	63.48	248.47	-20	43.48
9	1.5	299.36	247.71	-20	279.36
10	4.5	186.77	251.04	-20	166.77
11	7.5	85.96	259.03	-20	65.96
12	10.5	357.18	272.22	-20	337.18
13	13.5	280.66	291.13	+20	300.66
14	16.5	216.59	316.22	+20	236.59
15	19.5	165.12	347.91	+20	185.12
16	22.5	126.40	386.40	+20	146.40

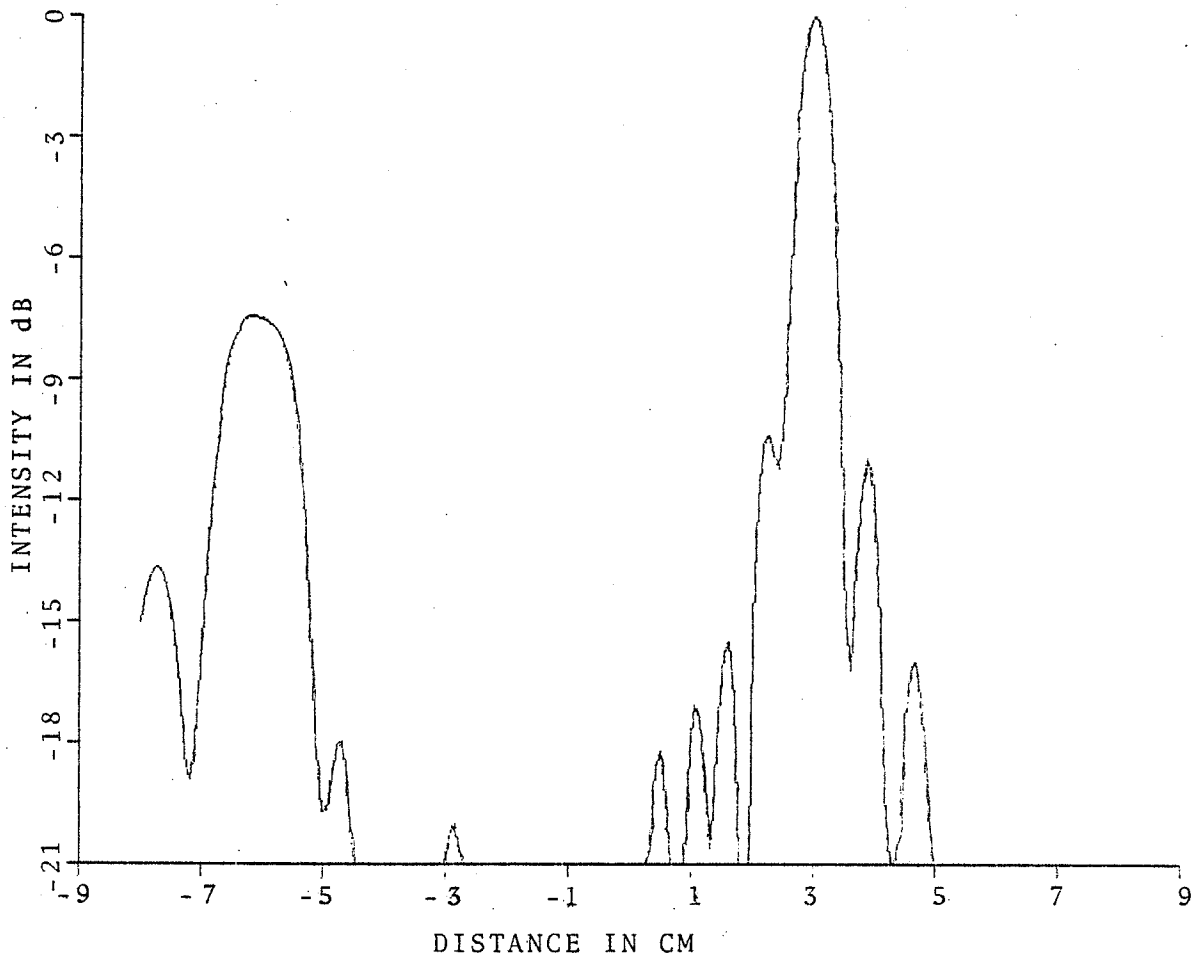

Figure 5.3 Intensity Profile with Shift

CHAPTER 6

RECOMMENDATIONS FOR FUTURE WORK

The most promising method of improving the performance of the array without decreasing the minimum spacing of the elements appears to be using nonuniformly spaced elements. The use of nonuniformly spaced elements has been shown to significantly reduce grating lobe levels for electromagnetic arrays [Lo, 1967], and, because of the similar wave nature of ultrasound, the same improvements can be expected for an ultrasonic hyperthermia array.

The difficulty in designing a nonuniformly spaced array is that there is no analytical method that will give the optimum spacing. As was noted by Lo [Lo, 1967], the only way of assuring that the optimum spacing is used is by finding the sidelobe height for all possible arrangements and choosing the spacing with the lowest sidelobe level.

APPENDIX A

FOURIER TRANSFORM METHOD PROGRAM

```
#BATCH
C  THIS PROGRAM CALCULATES AND PLOTS THE NEARFIELD PRESSURE
C  DISTRIBUTION PRODUCED BY A LINEAR ULTRASONIC PHASED ARRAY
C  USING THE FOURIER TRANSFORM METHOD.  THE INPUTS ARE THE ARRAY
C  TO FIELD POINT DISTANCE, NUMBER OF ELEMENTS, ELEMENT HEIGHT,
C  ELEMENT WIDTH, AND ELEMENT PHASINGS.  FOR THIS IMPLEMENTATION
C  THE ARRAY IS SAMPLED AT 1/3 MM SPACING AND INPUT DIMENSIONS ARE
C  ENTERED AS INTEGER NUMBERS OF SAMPLE POINTS.
C
      COMPLEX Y(256),X(128),D(256),A(128,129),PQ(20),CAK
      DIMENSION NES(128),NEF(128)
      DIMENSION ADAT(128),XM(130),YM(130)
      DATA NPX,NPXP3,NPXH,NPXHP1,NX,NPXP1/128,131,64,65,7,129/
      DATA NPY,NPYP3,NPYP2,NY,NPYHP1/256,259,258,8,129/
      DATA WVELGH/7.5/
      AK=2.0*3.1415926/WVELGH
      CAK=CMPLX(0.0,-AK)
C
C  INPUT ARRAY GEOMETRY.
C
      WRITE(6,98)
   98 FORMAT(' ENTER DISTANCE TO IMAGE PLANE (50 TO 500 MM)')
      READ(5,99)ZDIST
      ZDIST=ZDIST*3.
   99 FORMAT(F20.4)
      WRITE(6,102)
  102 FORMAT(' ENTER NUMBER OF ELEMENTS IN I2 FORM')
      READ(5,103)NE
  103 FORMAT(I2)
      WRITE(6,100)
  100 FORMAT(' ENTER HT OF ELEMENTS I3 FORM (ODD # OF POINTS)')
      READ(5,101)NH
  101 FORMAT(I3)
      WRITE(6,104)
  104 FORMAT(' ENTER ELEMENT WIDTH IN I3 (ODD NUMBER OF POINTS)')
      READ(5,101)NW
      WRITE(6,105)
  105 FORMAT(' ENTER DISTANCE BETWEEN ELEMENT CENTERS IN I3')
      READ(5,101)NS
      WRITE(6,322)
  322 FORMAT(' ENTER X COORDINATE OF FOCUS RELATIVE TO ARRAY',
     #' CENTER IN F FORMAT')
      READ(5,99)FOCUS
      FOCUS=FOCUS*3.
      XVAL=-FLOAT((NE-1)*NS)/2.
      DO 423 I=1,NE
      RDIST=SQRT((FOCUS-XVAL)**2+ZDIST**2)
      PHAS=AK*RDIST
      PQ(I)=CMPLX(COS(PHAS),SIN(PHAS))
      XVAL=XVAL+FLOAT(NS)
  423 CONTINUE
```

```
C
C  USE SEPARABILITY OF SURFACE VELOCITY IN X AND Y TO SPEED
C  TRANSFORM EVALUATION.  THE FIELD IS CALCULATED BY FINDING THE
C  PRESSURE PRODUCED BY ONE ELEMENT AND USING SUPERPOSITION TO
C  CALCULATE THE PRESSURE FOR THE WHOLE ARRAY.
C
C  FORM AND TRANSFORM X VELOCITY DISTRIBUTION.
C
      DO 1 I=1,NPX
    1 X(I)=CMPLX(0.,0.)
      NXBEG=(NPXP3-NW)/2
      NXEND=NXBEG+NW-1
      DO 2 J=NXBEG,NXEND
    2 X(J)=CMPLX(1.,0.)
      CALL FFT(X,NX,0)
C
C  FORM AND TRANSFORM Y VELOCITY DISTRIBUTION.
C
      DO 4 I=1,NPY
    4 Y(I)=CMPLX(0.,0.)
      NYBEG=(NPYP3-NH)/2
      NYEND=NYBEG+NH-1
      DO 5 J=NYBEG,NYEND
    5 Y(J)=CMPLX(1.,0.)
      CALL FFT(Y,NY,0)
C
C  FORM WEIGHTING MATRIX AND TRANSFORM.
C
      DO 50 I=1,NPX
      DO 51 J=1,NPYHP1
   51 A(I,J)=CMPLX(0.,0.)
   50 CONTINUE
      DO 61 I=1,NPX
      IF(I .GE. NXBEG .AND. I .LE. NXEND)GO TO 61
      CEE=NPXH-ABS(NPXHP1-FLOAT(I))
      ARG=SQRT(ZDIST**2+CEE**2)
      D(1)=CEXP(CAK*ARG)/ARG
      DO 62 J=2,NPYHP1
      IF(J .GE. NYBEG)D(J)=CMPLX(0.,0.)
      IF(J .GE. NYBEG)GO TO 59
      CEE=NPXH-ABS(NPXHP1-FLOAT(I))
      ETA=FLOAT(J-1)
      ARG=SQRT(ZDIST**2+CEE**2+ETA**2)
      D(J)=CEXP(CAK*ARG)/ARG
   59 INC=NPYP2-J
   62 D(INC)=D(J)
      CALL FFT(D,NY,0)
      DO 63 J=1,NPYHP1
   63 A(I,J)=D(J)
   61 CONTINUE
      DO 64 J=1,NPYHP1
   64 CALL FFT(A(1,J),NX,0)
C
C  MULTIPLY VELOCITY DISTIBUTION TRANSFORM BY WEIGHTING FUNCTION
C  TRANSFORM TO PERFORM CONVOLUTION.
```

```
C
      DO 6 I=1,NPX
      D(1)=X(I)*Y(1)*A(I,1)
      DO 7 J=2,NPYHP1
      D(J)=X(I)*Y(J)*A(I,J)
      IND=NPYP2-J
    7 D(IND)=D(J)
      CALL FFT(D,NY,1)
      DO 8 J=1,NPYHP1
    8 A(I,J)=D(J)
    6 CONTINUE
      DO 15 J=1,NPYHP1
   15 CALL FFT(A(1,J),NX,1)
      IF(NE .EQ. 1)GOTO 17
C
C  SHIFT FIELD PRODUCED BY ONE ELEMENT TO PRODUCE FIELD FOR AN
C  ARRAY OF ELEMENTS.
C
      MAX=(NE-1)*NS
      NSTART=-(MAX/2)
      NFINIS=NSTART+MAX
      DO 70 I=1,NPX
      NES(I)=1
      NEF(I)=NE
      IF(NSTART+I .LT. 1)NES(I)=2-(NSTART+I)/NS
   70 IF(NFINIS+I .GT. NPX)NEF(I)=NE-1-(NFINIS+I-NPXP1)/NS
      DO 74 J=1,NPYHP1
      DO 71 I=1,NPX
   71 D(I)=CMPLX(0.,0.)
      DO 72 I=1,NPX
      NST=NES(I)
      NFI=NEF(I)
      DO 73 K=NST,NFI
      IND=I+NSTART+(K-1)*NS
   73 D(I)=D(I)+A(IND,J)*PQ(K)
   72 CONTINUE
      DO 75 I=1,NPX
   75 A(I,J)=D(I)
   74 CONTINUE
C
C  DISPLAY PRESSURE FIELD.
C
      NP=NPX
      PDAMAX=1.E-10
      DO 17 I=1,128
   17 ADAT(I)=CABS(A(I,128))
      CALL PLOTS(0.0,7)
      DO 390 I=1,NP
  390 PDAMAX=AMAX1(ADAT(I),PDAMAX)
      DBPMAX=20.*ALOG10(PDAMAX)
      STEP=1/3.
      START=-21.33333
      DO 400 I=1,NP
      XM(I)=.1*(START+(I-1)*STEP)
      YM(I)=(-DBPMAX)+20.*ALOG10(ADAT(I)+1.E-5)
```

```
 400   IF(YM(I) .LT. -21.)YM(I)=-21.
       CALL SCALE(XM,9.0,NP,1)
       CALL AXIS(.5,1.,'DISTANCE (CM)',-13,9.,0.,XM(NP+1),XM(NP+2))
       CALL AXIS(.5,1.,'INTENSITY IN DB',15,7.,90.,-21.,3.)
       CALL PLOT(0.5,1.,-3)
       CALL LINE(XM,YM,NP,1,0,2)
       CALL PLOT(0.,0.,10)
       CALL PLOT(0.,0.,11)
       STOP
       END
C
C  THE SUBROUTINE FFT PERFORMS A ONE DIMENSIONAL FFT OR IFFT
C  USING ASSEMBLY LANGUAGE.  THE ARGUMENTS ARE THE COMPLEX DATA
C  VECTOR A, M WHERE 2**M IS THE FFT SIZE, AND OPT WHERE OPT=0
C  FOR AN FFT AND OPT=1 FOR AN IFFT.
C
       SUBROUTINE FFT(A,M,OPT)
       COMPLEX A(1),U,W,T
       INTEGER*4 S1(16),S2(16),S,OPT
       N = 2**M
#ASSM
          STM    0,S1
          LIS    1,8
          LR     2,1
          L      3,N
          SIS    3,2
          SLLS   3,3
          L      4,N
          SLLS   4,2
          LIS    5,0
          L      10,A
LOOP3     LR     6,4
LOOP4     CLR    5,6
          BTFS   8,JUMP1
          SR     5,6
          SRLS   6,1
          B      LOOP4
JUMP1     AR     5,6
          CLR    1,5
          BFC    8,JUMP2
          L      6,0(1,10)
          L      7,4(1,10)
          L      8,0(5,10)
          L      9,4(5,10)
          ST     6,0(5,10)
          ST     7,4(5,10)
          ST     8,0(1,10)
          ST     9,4(1,10)
JUMP2     BXLE   1,LOOP3
          LM     0,S1
#FORT
       PI = 3.1415926535
       S=-1
       IF(OPT.EQ.1)S=1
       DO 20 L = 1,M
```

```
      LE = 2**L
      LE1 = LE/2
      U = (1.,0.)
      W = CMPLX(COS(PI/LE1),S*SIN(PI/LE1))
#ASSM
          STM   0,S1
          STME  0,S2
          LE    0,U
          LE    2,U+4
          LIS   0,0
          LIS   1,8
          L     2,LE1
          SIS   2,1
          SLLS  2,3
          L     6,LE1
          SLLS  6,3
LOOP1     L     3,A
          AR    3,0
          L     4,LE
          SLLS  4,3
          L     5,N
          SIS   5,1
          SLLS  5,3
          AR    5,3
LOOP2     LE    4,0(3,6)
          LE    6,4(3,6)
          LER   8,4
          LER   10,6
          MER   4,0
          MER   6,2
          MER   8,2
          MER   10,0
          SER   4,6
          AER   10,8
          LE    6,0(3)
          LE    8,4(3)
          LER   12,6
          LER   14,8
          AER   12,4
          AER   14,10
          SER   6,4
          SER   8,10
          STE   6,0(3,6)
          STE   8,4(3,6)
          STE   12,0(3)
          STE   14,4(3)
          BXLE  3,LOOP2
          LE    4,W
          LE    6,W+4
          LER   8,6
          LER   10,6
          MER   8,2
          MER   10,0
          MER   0,4
          MER   2,4
```

```
          SER    0,8
          AER    2,10
          BXLE   0,LOOP1
          LME    0,S2
          LM     0,S1
#FORT
  20   CONTINUE
       IF(OPT .EQ. 0) GO TO 100
#ASSM
          STM    0,S1
          STME   0,S2
          L      1,A
          LIS    2,8
          L      3,N
          SIS    3,1
          SLLS   3,3
          AR     3,1
          L      4,N
          FLR    0,4
LOOP5     LE     2,0(1)
          LE     4,4(1)
          DER    2,0
          DER    4,0
          STE    2,0(1)
          STE    4,4(1)
          BXLE   1,LOOP5
          LME    0,S2
          LM     0,S1
#FORT
  100     CONTINUE
       RETURN
       END
#BEND
```

APPENDIX B

FRAUNHOFER APPROXIMATION METHOD PROGRAM

```
#BATCH
C  THIS PROGRAM CALCULATES AND PLOTS THE PRESSURE DISTRIBUTION
C  CALCULATED USING THE FRAUNHOFER APPROXIMATION.
C  THE PROGRAM IS WRITTEN FOR EQUALLY SPACED ELEMENTS OF
C  EQUAL WIDTHS.
      COMPLEX X(1024),RAI(16)
      DIMENSION XN(135),YM(135),XM(135)
C  ASSIGN CONSTANTS.
      DATA NE,SPAC,DX,FREQ,N,LOC/16,3.,.25,600.,1024,406/
      DATA FOCUSX,FOCUSZ,PLOTZ,NP/3000.,10000.,100.,133/
      SPACT=SPAC*FLOAT(NE-1)
      WAVE=1500./FREQ
      CAK=2.*3.14159265/WAVE
C  CREATE VECTOR REPRESENTING X CROSS SECTION OF ARRAY.
      DO 10 I=1,N
 10   X(I)=(0.,0.)
      XVAL=-SPACT/2.
      DO 20 J=1,NE
      LOC=LOC+12
C  PHASE ELEMENTS TO CREATE FOCUS AT (FOCUSX,0,FOCUSZ).
      RDIST=SQRT((FOCUSX-XVAL)**2+FOCUSZ**2)
      XVAL=XVAL+SPAC
      CAR=CAK*RDIST
      RAI(J)=CMPLX(COS(CAR),SIN(CAR))
      DO 30 K=1,10
      IT=LOC+K-1
      X(IT)=RAI(J)
  30  CONTINUE
  20  CONTINUE
C  TRANSFORM X VECTOR.
      CALL FFT(X,10,0)
C  ACCOUNT FOR NEGATIVE SIGN IN FRAUNHOFER APPROXIMATION
C  EQUATION.
      DO 40 I=1,67
      LOC=68-I
      XN(I)=CABS(X(LOC))
  40  CONTINUE
      DO 50 I=68,133
      LOC=1092-I
      XN(I)=CABS(X(LOC))
  50  CONTINUE
      XM(67)=0.
C  CALCULATE X LOCATIONS OF POINTS TO BE PLOTTED.
      DO 60 I=1,66
      XT=PLOTZ/SQRT((FLOAT(N)*DX/WAVE/FLOAT(I))**2-1)
      I1=67-I
      XM(I1)=-XT
      I2=67+I
      XM(I2)=XT
  60  CONTINUE
C  WEIGHT VALUES BY 1/R.
```

```
      DO 70 I=1,133
      XN(I)=XN(I)/SQRT(FOCUSZ**2+XM(I)**2)
   70 CONTINUE
C  GRAPH OUTPUT
C  PLOTTING ROUTINE
      CALL PLOTS(0.0,7)
      PDAMAX=0.
      DO 390 I=1,NP
  390 PDAMAX=AMAX1(XN(I),PDAMAX)
      DBPMAX=20.*ALOG10(PDAMAX)
      DO 400 I=1,NP
      YM(I)=(-DBPMAX)+20.*ALOG10(XN(I)+1.E-5)
  400 IF(YM(I) .LT. -21.)YM(I)=-21.
      CALL SCALE(XM,9.0,NP,1)
      CALL AXIS(.5,.5,'DISTANCE (CM)',-13,9.,0.,XM(NP+1),XM(NP+2))
      CALL AXIS(.5,.5,'INTENSITY IN DB',15,7.,90.,-21.,3.)
      CALL PLOT(0.5,0.5,-3)
      CALL LINE(XM,YM,NP,1,0,2)
      CALL PLOT(0.,0.,10)
      CALL PLOT(0.,0.,11)
      STOP
      END
C
C  THE SUBROUTINE FFT PERFORMS A ONE DIMENSIONAL FFT OR IFFT
C  USING ASSEMBLY LANGUAGE.  THE ARGUMENTS ARE THE COMPLEX DATA
C  VECTOR A, M WHERE 2**M IS THE FFT SIZE, AND OPT WHERE OPT=0
C  FOR AN FFT AND OPT=1 FOR AN IFFT. BECAUSE OF ITS LENGTH FFT IS
C  OMITTED HERE AND THE READER IS REFERRED TO APPENDIX A FOR
C  THE COMPLETE SUBROUTINE LISTING.
C
C     SUBROUTINE FFT(A,M,OPT)
#BEND
```

APPENDIX C

POINT RADIATOR METHOD PROGRAM

```
C  THIS PROGRAM CALCULATES AND PLOTS THE NEARFIELD PRESSURE
C  DISTRIBUTION PRODUCED BY A LINEAR ULTRASONIC PHASED ARRAY
C  USING THE POINT RADIATOR METHOD.  THIS PROGRAM ALLOWS FOR
C  VARIABLY SPACED ELEMENTS OF DIFFERENT WIDTHS.
C
      COMPLEX RAI(20),ACX(200),WT
      DIMENSION ADAT(200),FOCUS(3),SPAC(20),NWDTH(20),IB(4)
      DIMENSION XM(202),YM(202),START(3),DIFF(3)
      INTEGER*4 CHAR(3)
      DATA SPAC(1),SPACT,PDAMAX,PI/0.,0.,-1.,3.141592654/
      DATA CHAR(1),CHAR(2),CHAR(3)/'X','Y','Z'/
C
C  DATA IS ENTERED WITH DIMENSIONS IN MM.
C
      WRITE(6,10)
   10 FORMAT(' ENTER 1 FOR X-SCAN, 2 FOR Y-SCAN, OR 3 FOR Z-SCAN')
      READ(5,20)ITYPE
   20 FORMAT(I1)
      WRITE(6,30)
   30 FORMAT(' ENTER OPTION CODE OF 4 DIGITS, 1=YES, 0=NO',/,
     #' OPTIONS:VARIABLE MAGNITUDE,FOCUSED PHASE,VARIABLE SPACING'
     #/'          VARIABLE WIDTH')
      READ(5,40)ICODE
   40 FORMAT(I4)
      DO 50 I=1,4
   50 IB(I)=ICODE/10**(I-1)-ICODE/10**I*10
      WRITE(6,52)
   52 FORMAT(' ENTER FREQUENCY IN KHZ')
      READ(5,90)F
      WRITE(6,55)
   55 FORMAT(' ENTER NUMBER OF SAMPLE POINTS PER MM')
      READ(5,90)PPMM
      CAK=-2.*PI*F/1500./PPMM
      WRITE(6,57)
   57 FORMAT(' ENTER NUMBER OF POINTS TO BE PLOTTED IN I3')
      READ(5,58)NP
   58 FORMAT(I3)
      WRITE(6,60)
   60 FORMAT(' ENTER NUMBER OF ELEMENTS IN I2 FORM')
      READ(5,70)NE
   70 FORMAT(I2)
      WRITE(6,80)
   80 FORMAT(' ENTER ELEMENT HEIGHT (3 DB) IN MM (F FORMAT)')
      READ(5,90)T1
   90 FORMAT(F20.10)
      NH=2*INT(T1*PPMM/2.)
      IF(IB(1) .EQ. 1)GOTO 120
      WRITE(6,110)
  110 FORMAT(' ENTER ELEMENT WIDTH (3 DB) IN MM (F FORMAT)')
      READ(5,90)T1
      NW=T1*PPMM
```

```
 120  IF(IB(2) .EQ. 1)GOTO 170
      WRITE(6,130)
 130  FORMAT(' ENTER ELEMENT SPACING IN MM (F FORMAT)')
      READ(5,90)SPACE
 170  DO 290 I=1,NE
      RAI(I)=CMPLX(1.,0.)
      IF(IB(4) .EQ. 0 .AND. IB(3) .EQ. 1)GOTO 220
      T2=0.0
      IF(IB(3) .EQ. 1)GOTO 190
      WRITE(6,180)I
 180  FORMAT(' ENTER ELEMENT ',I2,' PHASE(DEG) IN F FORMAT')
      READ(5,90)T2
 190  T1=1.
      IF(IB(4) .EQ. 0)GOTO 210
      WRITE(6,200)I
 200  FORMAT(' ENTER ELEMENT ',I2,' MAGNITUDE IN F FORMAT')
      READ(5,90)T1
 210  RAI(I)=CMPLX(T1*COS(T2*.017453293),T1*SIN(T2*.017453293))
 220  IF(IB(1) .EQ. 0)NWDTH(I)=NW
      IF(IB(1) .EQ. 0)GOTO 260
      WRITE(6,230)I
 230  FORMAT(' ENTER WIDTH (3 DB) OF ELEMEMT',I2,' IN MM')
      READ(5,90)T1
      NWDTH(I)=T1*PPMM
 260  IF(IB(2) .EQ. 0)SPAC(I+1)=SPACE
      IF(IB(2) .EQ. 0)GOTO 280
      IF(I .NE. NE)WRITE(6,270)I
 270  FORMAT(' ENTER DISTANCE TO NEXT ELM CENTER AFTER ELM ',I2)
      IF(I .NE. NE)READ(5,90)SPAC(I+1)
 280  SPAC(I)=SPAC(I)*PPMM
      SPACT=SPACT+SPAC(I)
 290  CONTINUE
      DO 310 I=1,3
      WRITE(6,300)CHAR(I)
 300  FORMAT(' ENTER ',A1,' STARTING POINT IN MM (F FORMAT)')
      READ(5,90)TEMP
 310  START(I)=TEMP*PPMM
      WRITE(6,320)CHAR(ITYPE)
 320  FORMAT(' ENTER ',A1,' INCREMENT IN MM (F FORMAT)')
      READ(5,90)TEMP
      STEP=TEMP*PPMM
C
C  COORDINATES OF FOCAL POINT ARE SPECIFIED FOR PHASING ELEMENTS.
C
      IF(IB(3) .EQ. 0)GOTO 329
      DO 327 I=1,3,2
      WRITE(6,322)CHAR(I)
 322  FORMAT(' ENTER ',A1,' LOCATION OF FOCUS RELATIVE TO ARRAY',
     #' CENTER IN F FORMAT')
      READ(5,90)FOCUS(I)
      FOCUS(I)=FOCUS(I)*PPMM
 327  CONTINUE
      WRITE(6,3271)
 3271 FORMAT(' ENTER NUMBER OF BITS FOR QUANTIZATION IN I2')
      READ(5,70)IQ
```

```
      IQ=2**IQ
      XVAL=-SPACT/2.
      DO 328 I=1,NE
      XVAL=XVAL+SPAC(I)
      RDIST=SQRT((FOCUS(1)-XVAL)**2+FOCUS(3)**2)
      CAR=-CAK*RDIST
      IF(IQ .EQ. 1)GO TO 3278
      CAR=2.*PI*INT(.5+FLOAT(IQ)*CAR/(2.*PI))/FLOAT(IQ)
 3278 ANG=CAR*180./PI
      WRITE(6,90)ANG
      RAI(I)=RAI(I)*CMPLX(COS(CAR),SIN(CAR))
  328 CONTINUE
  329 CONTINUE
C
C  USE DO LOOPS TO CALCULATE THE CONTRIBUTION AT EACH FIELD POINT
C  FROM EACH ELEMENT POINT.
C
      DO 330 I=1,NP
  330 ACX(I)=CMPLX(0.,0.)
      XBEG=(-1.+SPACT+(FLOAT(NWDTH(1)+NWDTH(NE))/2.))/2.
      YBEG=FLOAT(NH-1)/2.
      EXSTAR=START(1)+XBEG
      EYSTAR=START(2)+YBEG
      IF(ITYPE .NE. 2)NH=NH/2
      DIFF(3)=START(3)
      DO 370 K=1,NE
      WT=RAI(K)
      EXSTAR=EXSTAR-SPAC(K)
      NW=NWDTH(K)
      DO 360 L=1,NW
      DIFF(1)=EXSTAR-L+1
      DO 350 M=1,NH
      DIFF(2)=EYSTAR-M+1
      DIFFTP=DIFF(ITYPE)
      DO 340 I=1,NP
      ARG=SQRT(DIFF(1)**2+DIFF(2)**2+DIFF(3)**2)
      CAKARG=CAK*ARG
      ACX(I)=ACX(I)+WT*CMPLX(COS(CAKARG)/ARG,SIN(CAKARG)/ARG)
      DIFF(ITYPE)=STEP+DIFF(ITYPE)
  340 CONTINUE
      DIFF(ITYPE)=DIFFTP
  350 CONTINUE
  360 CONTINUE
  370 CONTINUE
      DO 380 I=1,NP
  380 ADAT(I)=CABS(ACX(I))
C
C  A SPECIALIZED PLOTTING ROUTINE IS USED FOR DISPLAYING THE DATA.
C
      CALL PLOTS(0.0,7)
      DO 390 I=1,NP
  390 PDAMAX=AMAX1(ADAT(I),PDAMAX)
      DBPMAX=20.*ALOG10(PDAMAX)
      DO 400 I=1,NP
      XM(I)=(START(ITYPE)+(I-1)*STEP)/PPMM
```

```
      YM(I)=(-DBPMAX)+20.*ALOG10(ADAT(I)+1.E-50)
400   IF(YM(I) .LT. -21.)YM(I)=-21.
      CALL SCALE(XM,9.0,NP,1)
      CALL AXIS(0.5,0.5,'DIST (MM)',-9,9.0,0.0,XM(NP+1),XM(NP+2))
      CALL AXIS(0.5,0.5,'POWER (DB)',10,7.0,90.0,-21.,3.)
      CALL PLOT(0.5,0.5,-3)
      CALL LINE(XM,YM,NP,1,0,2)
      CALL PLOT(0.,0.,10)
      CALL PLOT(0.,0.,11)
      STOP
      END
```

APPENDIX D

EQUIDISTANT AREA METHOD PROGRAM

```
#BATCH
C  THIS PROGRAM CALCULATES AND PLOTS THE NEARFIELD PRESSURE
C  DISTRIBUTION PRODUCED BY AN ULTRASONIC LINEAR PHASED ARRAY
C  USING THE EQUIDISTANT AREA METHOD.
C
      DIMENSION PT(3),ADAT(200),XM(202),YM(202)
      COMPLEX AC,PQ(20),AS
      DATA PT(2)/0./
      DATA FREQ,PDAMAX/600.,1.E-10/
      NP=200
      STEP=.8
      START=-80.
      WRITE(6,430)
 430  FORMAT(' ENTER DELTA SIZE')
      READ(5,441)DELTA
 441  FORMAT(F20.10)
      AK=2*3.1415926536*FREQ/1500.
      CAK=-AK
      WRITE(6,98)
  98  FORMAT(' ENTER DISTANCE TO IMAGE PLANE (50 TO 500 MM)')
      READ(5,99)PT(3)
  99  FORMAT(F20.4)
      WRITE(6,102)
 102  FORMAT(' ENTER NUMBER OF ELEMENTS IN I2 FORM')
      READ(5,103)NE
 103  FORMAT(I2)
      WRITE(6,100)
 100  FORMAT(' ENTER ELEMENT HEIGHT IN F FORMAT')
      READ(5,99)HT
      WRITE(6,104)
 104  FORMAT(' ENTER ELEMENT WIDTH IN F FORMAT')
      READ(5,99)WI
      WRITE(6,105)
 105  FORMAT(' ENTER ELEMENT SPACING IN MM (F FORMAT)')
      READ(5,99)SP
      WRITE(6,322)
 322  FORMAT(' ENTER X COORDINATE OF FOCUS RELATIVE TO ARRAY',
     #' CENTER IN F FORMAT')
      READ(5,99)FOCUS
      XST=-SP*FLOAT(NE-1)/2.
      XVAL=XST
      DO 423 J=1,NE
      RDIST=SQRT((FOCUS-XVAL)**2+PT(3)**2)
      PHAS=AK*RDIST
      PQ(J)=CMPLX(COS(PHAS),SIN(PHAS))
      WRITE(6,450)PQ(J)
 450  FORMAT(2F10.4)
      XVAL=XVAL+SP
 423  CONTINUE
      Y1=-HT/2.
      Y2=HT/2.
```

```
      DO 1 I=1,NP
      PT(1)=STEP*I+START
      XVAL=XST
      AS=(0.,0.)
      DO 2 J=1,NE
      X1=XVAL-WI/2.
      X2=XVAL+WI/2.
      AC=(0.,0.)
C
C  FIELD CALCULATES THE FIELD AT ONE POINT DUE TO ONE ELEMENT.
C
      CALL FIELD(PT,X1,X2,Y1,Y2,CAK,DELTA,AC,NUM,0.,0.)
      AS=AS+PQ(J)*AC
      XVAL=XVAL+SP
   2  CONTINUE
      ADAT(I)=CABS(AS)
  1   CONTINUE
C
C  ROUTINE TO PLOT DATA.
C
C  PLOTTING ROUTINE
      CALL PLOTS(0.0,7)
      DO 390 I=1,NP
 390  PDAMAX=AMAX1(ADAT(I),PDAMAX)
      DBPMAX=20.*ALOG10(PDAMAX)
      DO 400 I=1,NP
      XM(I)=.1*(START+(I-1)*STEP)
      YM(I)=(-DBPMAX)+20.*ALOG10(ADAT(I)+1.E-5)
 400  IF(YM(I) .LT. -21.)YM(I)=-21.
      CALL SCALE(XM,9.0,NP,1)
      CALL AXIS(.5,1.,'DISTANCE (CM)',-13,9.,0.,XM(NP+1),XM(NP+2))
      CALL AXIS(.5,.5,'INTENSITY IN DB',15,7.,90.,-21.,3.)
      CALL PLOT(0.5,1.,-3)
      CALL LINE(XM,YM,NP,1,0,2)
      CALL PLOT(0.,0.,10)
      CALL PLOT(0.,0.,11)
      STOP
      END
C
C  FIELD IS A SUBROUTINE TO CALCULATE THE FIELD AT ONE POINT DUE
C  TO ONE ELEMENT.  THE ARGUMENTS OF FIELD ARE: THE COORDINATES
C  OF THE FIELD POINT PTμ THE LOCATIONS OF THE FOUR SIDE OF THE
C  ELEMENT X1, X2, Y1, AND Y2μ THE WAVE NUMBER CAKμ THE MAXIMUM
C  DISTANCE ERROR FOR EACH AREA DELTAμ THE ATTENUATION ATTENμ AND
C  THE PERCENT ABSORBTION PCTABS.  THE OUTPUTS OF FIELD ARE
C  THE COMPLEX PRESSURE ACMPLX AND THE NUMBER OF AREAS NECESSARY
C  NUM.
C
      SUBROUTINE FIELD(PT,X1,X2,Y1,Y2,CAK,DELTA,ACMPLX,NUM,
     #ATTEN,PCTABS)
      DIMENSION PT(3),DI(4),D(4)
      COMPLEX ACMPLX
C  FIND THE CLOSEST POINT ON THE ELEMENT TO THE FIELD POINT.
      CPX=PT(1)
      CPY=PT(2)
```

```
      IF(PT(1) .LT. X1)CPX=X1
      IF(PT(1) .GT. X2)CPX=X2
      IF(PT(2) .LT. Y1)CPY=Y1
      IF(PT(2) .GT. Y2)CPY=Y2
C  FIND THE RADIUS ASSOCIATED WITH THE CLOSEST POINT.
      RAD1=SQRT((PT(1)-CPX)**2+(PT(2)-CPY)**2)
C  FIND THE RADIUS TO THE FUTHEREST POINT ON THE ELEMENT (RMAX).
      D(4)=PT(1)-X1
      D(2)=X2-PT(1)
      D(1)=PT(2)-Y1
      D(3)=Y2-PT(2)
      DI(1)=SQRT(D(4)**2+D(1)**2)
      DI(2)=SQRT(D(2)**2+D(1)**2)
      DI(3)=SQRT(D(2)**2+D(3)**2)
      DI(4)=SQRT(D(4)**2+D(3)**2)
      RMAX=AMAX1(DI(1),DI(2),DI(3),DI(4))
      NUM=0
      AREA1=0.
C     SUM=0.
C
C  LOOP ON EQUIDISTANT AREAS.
C
 100  CONTINUE
      NUM=NUM+1
C  FIND DISTANCE TO INNER RING.
      PT32=PT(3)**2
      DIST=SQRT(RAD1**2+PT32)
C  FIND RADIUS ASSOCIATED WITH DELTA + DISTANCE.
      RAD2=SQRT((DIST+DELTA)**2-PT32)
C  STOP ITERATIONS WHEN FURTHEREST DISTANCE IS REACHED.
      IF(RAD2 .GT. RMAX)RAD2=RMAX
C  FIND AREA IN RAD1.
      IF(NUM .EQ. 1)GO TO 53
      CALL AREA(PT,RAD1,X1,X2,Y1,Y2,AREA1,DI,D)
C  REPEAT FOR RAD2.
  53  CALL AREA(PT,RAD2,X1,X2,Y1,Y2,AREA2,DI,D)
C  AREA IS (AREA FOR RAD2 - AREA FOR RAD1).
C  ADD AREAS FOUND FOR EACH RING.
      AR=AREA2-AREA1
      ARG=DIST+DELTA/2
      ACMPLX=ACMPLX+AR*CEXP(CMPLX(ATTEN,CAK*ARG))/ARG
C     SUM=SUM+AR
      IF(RAD2 .EQ. RMAX)GOTO 500
      RAD1=RAD2
      GOTO 100
 500  CONTINUE
C     WRITE(6,340)SUM,NUM
C340  FORMAT(F20.10,I10)
      RETURN
      END
C
C  SUBROUTINE AREA CALCULATES THE AREA AT A GIVEN RADIUS.
C
      SUBROUTINE AREA(PT,RAD,X1,X2,Y1,Y2,VAL,DI,D)
      DIMENSION PT(3),ISIDE(4),ICORN(4),DI(4),D(4)
```

```
C  FIND TOTAL AREA OF CIRCLE FIRST.
      RADSQ=RAD**2
      VAL=3.1415926536*RADSQ
C  FIND WHICH SIDES OF RECTANGLE ARE IN CIRCLE OF RADIUS RAD.
C     SIDE IS IN CIRC IF: 1) CORNER AT END OF SIDE IS IN CIRC
C     OR 2) CIRC EXTENDS PAST SIDE AND CENTER IS BETWEEN CORNERS.
C  FIND NUMBER OF CORNERS ARE INCLUDED IN RADIUS.
C  ICORN=1 FOR CORNER WITHIN CIRCLE, 0 FOR OUTSIDE.
      DO 20 I=1,4
      ICORN(I)=0
      ISIDE(I)=0
      IF(DI(I) .GE. RAD)GOTO 20
C  ADD TRIANGLAR AREA FOR EACH CORNER IN CIRCLE.
      ICORN(I)=1
      IF(I .GT. 1)D1=D(I-1)
      IF(I .EQ. 1)D1=D(4)
      D2=D(I)
      F1=SQRT(RADSQ-D2**2)-D1
      F2=SQRT(RADSQ-D1**2)-D2
      S=.5*SQRT(F1**2+F2**2)
      ROOT=SQRT(RADSQ-S**2)
      VAL=VAL+(.5*F1*F2+RADSQ*ATAN2(S,ROOT)-S*ROOT)
 20   CONTINUE
C  ISIDE=1 FOR ANY PART OF SIDE IN CIRCLE, 0 OTHERWISE.
      IF(ICORN(1)+ICORN(2) .GE. 1)ISIDE(1)=1
      IF(ICORN(2)+ICORN(3) .GE. 1)ISIDE(2)=1
      IF(ICORN(3)+ICORN(4) .GE. 1)ISIDE(3)=1
      IF(ICORN(1)+ICORN(4) .GE. 1)ISIDE(4)=1
      IF(PT(2) .LT. Y1 .OR. PT(2) .GT. Y2)GOTO 60
      IF(RAD .GT. D(4))ISIDE(4)=1
      IF(RAD .GT. D(2))ISIDE(2)=1
 60   IF(PT(1) .LT. X1 .OR. PT(1) .GT. X2)GOTO 130
      IF(RAD .GT. D(1))ISIDE(1)=1
      IF(RAD .GT. D(3))ISIDE(3)=1
130   CONTINUE
C  SUBTRACT AREA FOR SIDE IN CIRCLE.
      DO 70 I=1,4
      IF(ISIDE(I) .EQ. 0)GOTO 70
      ROOT=SQRT(RADSQ-D(I)**2)
      VAL=VAL-(RADSQ*ATAN2(ROOT,D(I))-D(I)*ROOT)
 70   CONTINUE
      RETURN
      END
#BEND
```

APPENDIX E

RECTANGULAR RADIATOR METHOD PROGRAM

```
C  THIS PROGRAM CALCULATES AND PLOTS THE NEARFIELD PRESSURE
C  DISTRIBUTION PRODUCED BY AN ULTRASONIC LINEAR PHASED ARRAY
C  USING THE RECTANGULAR RADIATOR METHOD. THIS PROGRAM ALLOWS
C  FOR VARIABLY SPACED ELEMENTS. THE RECTANGULAR RADIATOR
C  APPROXIMATION IS USED BY SUBSTITUTING THE INDICATED
C  STATEMENTS.
C
      COMPLEX RAI(150),ACMPLX(300),WT,EXPARG,TEMP
      DIMENSION ADAT(300),SPAC(150),WGHT(50)
      DIMENSION DIFF(3),IB(5),XM(302),YM(302)
      DATA SPAC(1),SPACT,PDAMAX/0.,0.,1.E-10/
      DATA RHO,PI/1.,3.1415926536/
C
C  DATA ENTRY SECTION.
C  ELEMENT SIZES ARE ENTERED IN MM.
C
      WRITE(6,10)
   10 FORMAT(' ENTER NUMBER OF FIELD POINTS IN I3(UP TO 300)')
      READ(5,11)NP
   11 FORMAT(I3)
      WRITE(6,25)
   25 FORMAT(' ENTER FREQUENCY IN KHZ')
      READ(5,90)FREQ
      WRITE(6,27)
   27 FORMAT(' ENTER FARFIELD CONSTANT')
      READ(5,90)FAR
      MINHD2=5.
      WAVE=1500./FREQ
      PIDW=PI/WAVE
      CAK=2.*PIDW
      WRITE(6,28)
   28 FORMAT(' ENTER ATTENUATION AT 1MHZ IN NEPERS/CM ')
      READ(5,90)ATTEN
      ATTEN=ATTEN*(FREQ/1000.)**1.1
      WRITE(6,21)ATTEN
   21 FORMAT(' ATTENUATION AT OPERATING FREQ IS ',F8.6,' NEP/CM')
      ATTEN=ATTEN/10.
      WRITE(6,30)
   30 FORMAT(' ENTER OPTION CODE OF 5 DIGITS, 1=YES, 0=NO',/,
     #' OPTIONS:VARIABLE MAGNITUDE,FOCUSED PHASE,VARIABLE SPACING'
     #/'    VARIABLE WIDTH,VERT GAUSSIAN SHAPE')
      READ(5,40)ICODE
   40 FORMAT(I5)
C  ICODE IS THE OPTION CODE.
C  DECODE ICODE INTO 6 IB'S: 1=YES, 0=NO.
      DO 50 I=1,5
   50 IB(I)=ICODE/10**(I-1)-ICODE/10**I*10
      WRITE(6,60)
   60 FORMAT(' ENTER NUMBER OF ELEMENTS IN I3 FORM')
      READ(5,11)NE
      WRITE(6,80)
```

```
   80  FORMAT(' ENTER ELEMENT HEIGHT (3 DB) IN MM (F FORMAT)')
       READ(5,90)HT
   90  FORMAT(F20.5)
C   SINCE HT IS 3 DB HEIGHT FOR GAUSSIAN, INCREASE HT SO COMPLETE
C   GAUSSIAN CURVE CAN BE REPRESENTED.
       IF(IB(1) .EQ. 1)HT=2.4*HT
       IF(IB(2) .EQ. 1)GOTO 120
       WRITE(6,110)
  110  FORMAT(' ENTER ELEMENT WIDTH IN MM (F FORMAT)')
       READ(5,90)WIDTH
  120  IF(IB(3) .EQ. 1)GOTO 170
       WRITE(6,130)
  130  FORMAT(' ENTER ELEMENT SPACING IN MM (F FORMAT)')
       READ(5,90)SPACE
C   LOOP ON NUMBER OF ELEMENTS TO GET SPACES AND PHASES.
  170  DO 290 I=1,NE
       RAI(I)=CMPLX(1.,0.)
       IF(IB(5) .EQ. 0 .AND. IB(4) .EQ. 1)GOTO 220
       T2=0.0
       IF(IB(4) .EQ. 1)GOTO 190
       WRITE(6,180)I
  180  FORMAT(' ENTER ELEMENT ',I2,' PHASE(DEG) IN F FORMAT')
       READ(5,90)T2
  190  T1=1.
       IF(IB(5) .EQ. 0)GOTO 210
       WRITE(6,200)I
  200  FORMAT(' ENTER ELEMENT ',I2,' MAGNITUDE IN F FORMAT')
       READ(5,90)T1
  210  RAI(I)=CMPLX(T1*COS(T2*.017453293),T1*SIN(T2*.017453293))
  220  CONTINUE
       IF(IB(3) .EQ. 0)SPAC(I+1)=SPACE
       IF(IB(3) .EQ. 0)GOTO 280
       IF(I .NE. NE)WRITE(6,270)I
  270  FORMAT(' ENTER DISTANCE TO NEXT ELM CENTER AFTER ELM ',I2)
       IF(I .NE. NE)READ(5,90)SPAC(I+1)
  280  SPACT=SPACT+SPAC(I)
  290  CONTINUE
C   GET STARTING POINT AND INCREMENTS.
       WRITE(6,300)
  300  FORMAT(' ENTER Z DIST FOR FOCUS AND PLOT IN MM (F FORMAT)')
       READ(5,90)ZDIST
       WRITE(6,301)
  301  FORMAT(' ENTER X STARTING POINT IN MM (F FORMAT)')
       READ(5,90)START
       WRITE(6,312)
  312  FORMAT(' ENTER X INCREMENT IN MM (F FORMAT)')
       READ(5,90)STEP
       IF(IB(4) .EQ. 0)GOTO 329
       WRITE(6,322)
  322  FORMAT(' ENTER X COORDINATE OF FOCUS RELATIVE TO ARRAY',
      #' CENTER IN F FORMAT')
       READ(5,90)FOCUS
       WRITE(6,3271)
 3271  FORMAT(' ENTER NUMBER OF BITS FOR QUANTIZATION IN I2')
       READ(5,3272)IQ
```

```
 3272 FORMAT(I2)
      IQ=2**IQ
C  CALCULATE PHASES FOR ELEMENTS TO ACHIEVE A FOCUS.
      XVAL=-SPACT/2.
      DO 328 I=1,NE
      XVAL=XVAL+SPAC(I)
      RDIST=SQRT((FOCUS-XVAL)**2+ZDIST**2)
      CAR=CAK*RDIST
      IF(IQ .EQ. 1)GO TO 3278
      CAR=2.*PI*INT(.5+FLOAT(IQ)*CAR/(2.*PI))/FLOAT(IQ)
 3278 CONTINUE
      RAI(I)=RAI(I)*CMPLX(COS(CAR),SIN(CAR))
 328  CONTINUE
 329  CONTINUE
C  ININTIALIZE DATA VECTOR.
      DO 330 I=1,NP
 330  ACMPLX(I)=CMPLX(0.,0.)
      DO 331 I=1,50
 331  WGHT(I)=1.
C  CALCULATE FIELD.
      DIFF(1)=START+(SPACT+WIDTH)/2.
      DIFF(2)=0.
      SNE=DIFF(1)
      NH=2+INT(HT/SQRT(WAVE*ZDIST/FAR))
      NHD2=NH/2
      IF(NHD2 .LT. MINHD2)NHD2=MINHD2
      YINC=HT/FLOAT(NHD2*2)
      CNSTY=PIDW*YINC
      IF(IB(1) .EQ. 0)GO TO 335
C  LOOP TO CLACULATE GAUSSIAN WEIGHTINGS.
      S=0.
      DO 334 I=1,NHD2
      WGHT(I)=EXP(-8.*(YINC*(-.5+FLOAT(I))/HT)**2)
      S=S+WGHT(I)
 334  CONTINUE
      S=2.*FLOAT(NHD2)/S
      DO 336 I=1,NHD2
 336  WGHT(I)=WGHT(I)*S
 335  DIFF(2)=DIFF(2)+YINC/2.
      NW=1+INT(WIDTH/SQRT(WAVE*ZDIST/FAR))
      XINC=WIDTH/FLOAT(NW)
      CNSTX=PIDW*XINC
      DO 370 K=1,NE
      DIFF(1)=DIFF(1)-SPAC(K)
      IF(K .EQ. 1)DIFF(1)=DIFF(1)-XINC/2.
      WT=RAI(K)*CMPLX(XINC*YINC,0.)
      SNH=DIFF(2)
      SNW=DIFF(1)
      DO 360 L=1,NW
      SNXP=DIFF(1)
      DO 350 M=1,NHD2
      DO 341 IX=1,NP
      ARG=SQRT(DIFF(1)**2+DIFF(2)**2+ZDIST**2)
      XARG=CNSTX*DIFF(1)/ARG
C  FOR THE RECTANGULAR RADIATOR APPROXIMATION, THE COMMENTED
```

```
C  STATEMENTS FOLLOWING ARE SUBSTITUTED FOR THE TWO STATEMENTS
C  THAT DIRECTLY FOLLOW.
C     XARG2=XARG**2
C     XARG4=XARG2**2
C     SINCX=(1.-.133563936*XARG2+.32811761E-2*XARG4)/
C    #(1.+.331027317E-1*XARG2+.4649838E-3*XARG4)
      SINCX=1.
      IF(ABS(XARG) .GT. .0001)SINCX=SIN(XARG)/XARG
C  THE TWO PRECEEDING STATEMENTS ARE NOT USED WITH THE
C  APPROXIMATION METHOD.
      YARG=CNSTY*DIFF(2)/ARG
      SINCY=1.
      IF(ABS(YARG) .GT. .0001)SINCY=SIN(YARG)/YARG
      EXPARG=CEXP(CMPLX(-ARG*ATTEN,-ARG*CAK))
      TEMP=EXPARG*WT*CMPLX(WGHT(M)*SINCX*SINCY/ARG,0.)
      ACMPLX(IX)=ACMPLX(IX)+TEMP
      DIFF(1)=DIFF(1)+STEP
 341  CONTINUE
      DIFF(1)=SNXP
      DIFF(2)=DIFF(2)+YINC
 350  CONTINUE
      DIFF(2)=SNH
      DIFF(1)=DIFF(1)-XINC
 360  CONTINUE
      DIFF(1)=SNW
 370  CONTINUE
      DIFF(1)=SNE
      DIFF(2)=0.
      DO 380 I=1,NP
      ADAT(I)=CABS(ACMPLX(I))
 380  CONTINUE
C  PLOTTING ROUTINE
      CALL PLOTS(0.0,7)
      DO 390 I=1,NP
 390  PDAMAX=AMAX1(ADAT(I),PDAMAX)
      DBPMAX=20.*ALOG10(PDAMAX)
      DO 400 I=1,NP
      XM(I)=.1*(START+(I-1)*STEP)
      YM(I)=(-DBPMAX)+20.*ALOG10(ADAT(I)+1.E-5)
      IF(YM(I) .LT. -21.)YM(I)=-21.
 400  CONTINUE
      CALL SCALE(XM,9.0,NP,1)
      CALL AXIS(.5,1.,'DISTANCE (CM)',-13,9.,0.,XM(NP+1),XM(NP+2))
      YM(NP+1)=-21.
      YM(NP+2)=3.
      CALL AXIS(0.5,1.,'INTENSITY',9,7.0,90.0,YM(NP+1),YM(NP+2))
      CALL PLOT(0.5,1.,-3)
      CALL LINE(XM,YM,NP,1,0,2)
      CALL PLOT(0.,0.,10)
      CALL PLOT(0.,0.,11)
      STOP
      END
```

REFERENCES

E. M. Arase, 'Mutual Radiation Impedance of Square and Rectangular Pistons in a Rigid Infinite Baffle,' J. Acoust. Soc. Am. 36, 1521-1525 (1964).

P. J. Benkesser, 'Investigation of Linear Phased Arrays for Hyperthermia Applications,' M. S. thesis, University of Illinois, Urbana, Illinois (1983).

D. S. Burnett and W. W. Soroka, 'Tables of Rectangular Piston Radiation Impedance Functions with Application to Sound Transmission Loss through Deep Aperatures,' J. Acoust. Soc. Am. 51, 1618-1623 (1972).

D. A. Christensen and C. H. Darney, 'Hyperthermia Production for Cancer Therapy: A Review of Fundamentals and Methods,' J. Microwave Power 16, 89-105, (1981).

A. Freedman, 'Sound Field of a Rectangular Piston,' J. Acoust. Soc. Am. 32, 197-209 (1960).

K. Hynynen, D. J. Watmough and J. R. Mallard, 'Design of Ultrasonic Transducers for Local Hyperthermia,' Ultrasound in Med. and Biol., 7, 397-402 (1981).

L. E. Kinsler, A. R. Frey, A. B. Coppens and J. V. Sanders, Fundamentals of Acoustics (John Wiley and Sons, New York, 1982).

P. P. Lele, 'Induction of Deep, Local Hyperthermia by Ultrasound and Electromagnetic Fields,' Radiation and Environmental Biophysics, 17, 205-217 (1980).

O. A. Lindemann, 'Radiation Impedance of a Long Narrow Rectangular Piston in a Plane Baffle,' J. Acoust. Soc. Am. 52, 1045-1048 (1971).

A. V. Oppenheim and R. W. Schafer, Digital Signal Processing, (Prentice-Hall, Inc., Englewood Cliffs, New Jersey, 1975).

H. Stenzel, 'Die Akustiche Strahlung der Kolbenmembran,' Acoustica 2, 263-281 (1952).

P. R. Stepanishen and K. C. Benjamin, 'Forward and Backward Projection of Acoustic Fields using FFT Method,' J. Acoust. Soc. Am. 71, 803-812, (1982).

G. W. Swenson, Jr., and W. E. Johnson, 'Radiation Impedance of a Rigid Square Piston in an Infinite Baffle,' J. Acoust. Soc. Am. 24, 84 (1952).

E. G. Williams and J. D. Maynard, 'Numerical Evaluation of the Rayleigh Integral for Planar Radiators using the FFT,' J. Acoust. Soc. Am. 72, 2020-2030 (1982).

J. Zemanek, 'Beam Behavior within the Nearfield of a Vibrating Piston,' J. Acoust. Soc. Am. 49, 181-191 (1970).